Divergence of TORC1-mediated Stress Response Leads to Novel Acquired Stress Resistance in a Pathogenic Yeast

Jinye Liang[^1], Christopher E. Youngstrom[1], Bin Z. He[^1]

[1]Biology Department, University of Iowa, Iowa City, IA 52242

[^]Correspondence should be addressed to
Bin Z. He, bin-he@uiowa.edu
Jinye Liang, jinye-liang@uiowa.edu

Running title: Evolution of acquired stress resistance for H_2O_2 in yeasts

Keywords: acquired stress resistance, gene regulatory evolution, phosphate starvation, oxidative stress, opportunistic yeast pathogen, TORC1, stress response

Abstract

Acquired stress resistance (ASR) enables organisms to prepare for environmental changes that frequently occur after an initial stressor. However, the mechanisms by which stress response networks are rewired to upregulate genes in anticipation of a stimulus are not well understood. In this study, we discovered that a short phosphate starvation induces oxidative stress response (OSR) genes in the pathogenic yeast *C. glabrata* and protects it against a severe H_2O_2 stress; the same treatment, however, provides little benefit in the low pathogenic-potential relative, *S. cerevisiae*. The ASR involves the same transcription factors (TFs) as the OSR, but with different combinatorial logics. We show that Target-of-Rapamycin Complex 1 (TORC1) is differentially inhibited by phosphate starvation in the two species and contributes to the ASR via its proximal effector, Sch9. Therefore, evolution of the phosphate starvation-induced ASR involves the rewiring of TORC1's response to phosphate limitation and the repurposing of TF-target gene networks for the OSR using new regulatory logics.

Introduction

Acquired stress resistance (ASR) is the phenomenon where organisms exposed to a non-lethal primary stress become more resistant to a secondary severe stress of the same or a different type (Lu *et al.* 1993; Leroi *et al.* 1994; Lou and Yousef 1997; Durrant and Dong 2004; Scholz *et al.* 2005; Hecker *et al.* 2007). Widely observed across kingdoms of life, ASR is believed to provide a survival advantage in environments with predictable changes. For example, it was shown in *S. cerevisiae* that stressors occurring early during fermentation, e.g., heat and ethanol, have a strong protective effect against stresses that occur later, such as oxidative stress, while the reverse is not true (Mitchell *et al.* 2009). This asymmetry in cross-stress protection suggests that ASR is not simply a general stress response but rather represents an adaptive anticipatory response, enabling cells to predict and survive future challenges. A natural prediction is that ASR must be adapted to the specific stress patterns organisms encounter in their environments, leading to divergence between species.

Despite the potential role of ASR in adaptation, we know little about its evolution. ASR is known to have biochemical, post-translational or transcriptional mechanisms (Davies 2016; Goulev *et al.* 2017). At the transcriptional level, studies in *S. cerevisiae* showed that ASR does not rely on a single, all-purpose program; instead, genes involved in ASR are regulated in a stress-specific manner (Gasch *et al.* 2000). Furthermore, ASR against the same secondary stress is dependent on distinct genes that are regulated by different types of primary stresses (Berry *et al.* 2011). Such stress-specific regulation enables mutations to target specific contexts and avoid pleiotropic effects, thereby facilitating the evolution of ASR. However, few studies dissected ASR in closely related species. Previous studies on ASR in yeasts, for example, have primarily focused on comparing *S. cerevisiae* with distantly related species, such as *C. albicans* and *S. pombe*, which are estimated to have diverged from the baker's yeast ~200 and ~500 million years ago (Chen *et al.* 2003; Rodaki *et al.* 2009; Rhind *et al.* 2011; Shen *et al.* 2018; Brown *et al.* 2020). These substantial evolutionary distances, coupled with the whole genome duplication (WGD) event specific to *S. cerevisiae*, significantly hindered our ability to discern the evolutionary alterations behind ASR divergence.

In this study, we focused on the more closely related *S. cerevisiae* and *C. glabrata*, both of which are post-WGD and share more than 90% of their genes with one-to-one orthologs (Dujon *et al.* 2004). Even though *C. glabrata* is evolutionarily close to *S. cerevisiae*, it is distinguished by its ability to colonize and infect humans (Kumar *et al.* 2019; Zakhem *et al.* 2021). As one of the most frequent causes for Candidiasis, it shares many phenotypic traits with the distantly related pathogen, *C. albicans*, including high resistance to host-associated stresses such as the oxidative stress (Fidel *et al.* 1999; Brunke and Hube 2013). In fact, it exhibits the highest resistance to H_2O_2 in a broad phylogenetic survey of fungi (Nikolaou *et al.* 2009). Apart from oxidative stress, host immune systems also use other stressors, such as nutrient limitation, to kill invading microbes (Seider *et al.* 2014). Given the array of challenges they encounter, it is probable that yeast pathogens such as *C. glabrata* evolved anticipatory responses to help them prepare for impending stresses (Brown *et al.* 2020). Interestingly, we and others found that *C. glabrata, C. albicans* and a more distantly related pathogen, *Cryptococcus neoformans*, all have an expanded phosphate starvation (PHO) response compared with that in *S. cerevisiae*,

71 including the induction of oxidative stress response (OSR) genes (Ikeh *et al.* 2016; He *et al.*
72 2017; Lev *et al.* 2017). As an essential macronutrient, fungal cells must acquire phosphate from
73 the environment. Emerging evidence suggests that responses to phosphate limitation play a
74 crucial role in the host-fungal interaction. First, a defective PHO pathway, either by deleting the
75 transcription factor (TF) *PHO4* or the high affinity phosphate transporter *PHO84*, leads to
76 reduced virulence and survival for *C. albicans* inside macrophages and animal models (Ikeh *et*
77 *al.* 2016, 2017; Liu *et al.* 2017, 2018). Second, two clinical isolates of *C. albicans* exhibit
78 enhanced virulence in a phosphate-dependent manner in both a *C. elegans* and a mouse model
79 of infection (Romanowski *et al.* 2012). Third, several PHO genes were found to be upregulated
80 in phagocytosed *C. glabrata* cells, suggesting that yeast cells experience phosphate limitation
81 inside the phagosome (Fig. S1) (Rai *et al.* 2021).
82 We found in this study that a short-term phosphate starvation led to the induction of at
83 least 15 OSR genes and enhanced the survival of *C. glabrata* against a severe H_2O_2 stress. The
84 same treatment had little to no effect in the related *S. cerevisiae*. Using transcriptional profiling,
85 genetic perturbations, reporter and survival assays, we identified key players in the network
86 underlying the ASR, including the catalase gene *CTA1*, transcription factors (TFs) Msn4 and
87 Skn7 and homolog of the Greatwall kinase, Rim15. We found that phosphate limitation quickly
88 and strongly suppressed the Target-of-Rapamycin Complex 1 (TORC1) in *C. glabrata* but not in
89 *S. cerevisiae*; the proximal effector Sch9 was also shown to contribute to the ASR in the former
90 species, strongly implicating TORC1 as a major contributor to the divergence in ASR. In
91 summary, our results identified a key signaling-TF-effector gene subnetwork underlying the
92 divergent ASR phenotype and thereby provides a concrete example of ASR evolution.

93 ## Results

94 **Phosphate starvation provides strong acquired resistance for H_2O_2 in *C. glabrata* but not**
95 **in *S. cerevisiae***

96 Based on the evidence linking phosphate to oxidative stress and virulence in *C. glabrata* and *C.*
97 *albicans*, we asked whether phosphate starvation could provide acquired resistance for severe
98 H_2O_2 stress in *C. glabrata* vs the related *S. cerevisiae*. To answer this question, wild type cells
99 from both species were subjected to 45 minutes of phosphate starvation, followed by a severe
100 H_2O_2 challenge (Fig. 1A). We designed the experiment to be able to compare the ASR effect
101 between species despite differences in their basal resistance level to H_2O_2, which affects the
102 magnitude of ASR (Berry and Gasch 2008). Through titration, we found that 100 mM and 10mM
103 H_2O_2 resulted in a similar ~2.5% survival in *C. glabrata* and *S. cerevisiae*, respectively (Fig.
104 S2A, $P = 1$). Using these concentrations as the secondary stress, we found that phosphate
105 starvation greatly enhanced the survival of *C. glabrata* after the H_2O_2 stress (Fig. 1B) but had no
106 detectable effect in *S. cerevisiae* (Fig. 1C). A quantitative colony forming unit (CFU) assay
107 confirmed this (Fig. 1D, $P = 0.0039$ and 0.37 in *C. glabrata* and *S. cerevisiae*, respectively). To
108 quantify the magnitude of ASR, we defined ASR-score as the fold increase in survival due to the
109 primary stress treatment, i.e., the ratio between the survival rates with (r') and without (r) the
110 primary stress. Using this definition, we found a 45-minute phosphate starvation led to an ASR-
111 score of 3.4 in *C. glabrata* (95% CI: [2.66, 4.26]), compared with 1.3 in *S. cerevisiae* (95% CI:

112 [0.90, 1.63]). To comprehensively test the relationship between phosphate starvation and ASR
113 for oxidative stress, we altered both the severity of the secondary stress and the length of the
114 primary stress and asked how this affected ASR in both species. We found that more severe
115 secondary stress (higher [H_2O_2]) led to stronger ASR in *C. glabrata* but not in *S. cerevisiae* at
116 the concentrations tested (Fig. S2B). When we increased the primary phosphate starvation
117 treatment to 90 and 135 minutes, we observed a stronger ASR in *C. glabrata* (ASR-scores =
118 111 and 170, $P < 0.05$ after Bonferroni correction, Fig. S2C). A similar trend was observed in *S.*
119 *cerevisiae* (ASR-score = 11 and 22) but didn't reach statistical significance (Bonferroni-
120 corrected $P = 0.7$ and 0.5).

121 We also wondered whether the ASR for H_2O_2 is systematically different between the two
122 species or whether phosphate starvation represents a distinct case of divergence. To answer
123 this question, we tested two common stressors, i.e., heat shock and glucose starvation, and
124 found that both led to ASR at a similar level between the two species (Fig. S3). Therefore, we
125 conclude that *C. glabrata* and *S. cerevisiae* diverged particularly in the phosphate starvation-
126 induced ASR for H_2O_2, where *C. glabrata* showed a strong ASR while the same primary stress
127 elicited a much weaker effect in *S. cerevisiae* only after prolonged phosphate starvation.

128 **Oxidative stress response genes were induced under phosphate starvation in *C. glabrata***

129 One potential mechanism for the observed ASR in *C. glabrata* is that phosphate starvation led
130 to the induction of oxidative stress response (OSR) genes during the primary stress (Fig. 2A).
131 To test this, we curated a set of H_2O_2-response genes in the well-studied *S. cerevisiae*, where
132 four TFs – Yap1, Skn7, Msn2 and Msn4 – induce a set of antioxidants, proteases, chaperones
133 and other genes to scavenge ROS and mitigate ROS-induced damages (Fig. 2B) (Lee *et al.*
134 1999; Hasan *et al.* 2002). Using this reference set (Table S1), we identified their orthologs in *C.*
135 *glabrata* and asked if they were induced during phosphate starvation. To do so, we profiled the
136 transcriptional response at 1 hour of phosphate starvation in *C. glabrata* and compared it with
137 the response to the same treatment in *S. cerevisiae* from (Zhou and O'Shea 2011). Of the 29
138 genes tested, 15 were significantly induced by at least two-fold in *C. glabrata* (FDR < 0.05),
139 compared with three in *S. cerevisiae* (Fig. 2C-F). These include antioxidant genes such as
140 *CTA1*, *PRX1*, *SOD1* and *SOD*2. Induction of these OSR genes could lead to enhanced ROS
141 scavenging and protection against oxidative damages in *C. glabrata*, consistent with its stronger
142 ASR effect (Jamieson 1998; Mason *et al.* 2005; Welker *et al.* 2010; Reichmann *et al.* 2018).
143 Interestingly, one of the four TFs mentioned above, Msn4, was strongly induced in *C. glabrata*
144 but not in *S. cerevisiae* (Fig. 2F). This and the fact that several of the OSR genes above were
145 known to be dependent on Msn2 and Msn4 in *S. cerevisiae*, including *CTT1* (homolog of *CTA1*),
146 *SOD2*, *TFS1, HSP12, HSP42,* and *HSP104*, led us to hypothesize that Msn4 contributes to their
147 up-regulation during phosphate starvation (Martínez-Pastor *et al.* 1996; Moskvina *et al.* 1998;
148 Hasan *et al.* 2002).

149 ***CTA1* is required for the ASR for H_2O_2 but not during phosphate starvation in *C. glabrata***

150 To test the hypothesis that the induction of OSR genes contributed to the ASR, we focused on
151 *CTA1*, which has a well-established role in the resistance to H_2O_2 in *C. glabrata* (Cuéllar-Cruz *et*
152 *al.* 2008). We first validated its induction using qRT-PCR and found *CTA1* to be ~3 fold induced
153 after 45 minutes of phosphate starvation (Fig. 3A). To confirm that protein levels increased

154 concordantly with mRNA, we endogenously tagged *CTA1* with GFP. This recombinant strain
155 had no defect in H_2O_2 resistance or growth (Fig. S4A). As expected based on the mRNA levels,
156 Cta1-GFP levels continued to increase during phosphate starvation as measured by flow-
157 cytometry (Fig. 3B). We next asked if *CTA1* was required for the phosphate starvation-induced
158 ASR in *C. glabrata*. We created a *cta1*Δ strain and compared its ASR phenotype with the wild
159 type using H_2O_2 concentrations that resulted in a similar basal survival rate. We found loss of
160 *CTA1* largely abolished the phosphate starvation-induced ASR for H_2O_2 (Fig. 3C). Quantitative
161 CFU assays revealed a residual ASR effect in *cta1*Δ (ASR-score = 1.5, 95% CI [1.2, 1.8], P =
162 0.016), which was much lower than that in the wild type strain (ASR-score = 9.8, 95% CI [5.5,
163 15], P = 0.016) (Fig. 3D). Interestingly, we found that while *CTA1* is crucial for the phosphate
164 starvation-induced ASR for H_2O_2, its role was less critical with a mild H_2O_2 used as the primary
165 stress (Fig. S4B). This result showed that the genetic basis for ASR is highly variable and
166 dependent on the primary stress (Berry *et al.* 2011).
167 The induction of *CTA1* or other OSR genes in *C. glabrata* under phosphate starvation
168 may either serve the primary stress and have an unintended benefit during the secondary
169 stress, or it may specifically serve the secondary stress and have neutral or even detrimental
170 effects during the primary stress. The latter was proposed as a key criterion for determining if a
171 cross-regulation pattern forms an adaptive anticipatory response (Mitchell *et al.* 2009). To
172 determine if the induction of *CTA1* and potentially other OSR genes under phosphate starvation
173 fulfills this criterion, we asked if *CTA1* was required under phosphate starvation. We found that
174 deletion of *cta1*, or the main TF for the canonical OSR, *yap1*, showed no defect in phosphate
175 limited conditions, while a strain lacking Pho4 and thus unable to induce the PHO response had
176 severe defects as expected (Fig. S4C, D). Therefore, we conclude that the induction of *CTA1*
177 primarily serves the secondary H_2O_2 stress.

178 **Msn4 and Skn7 contribute to *CTA1* induction during phosphate starvation in *C. glabrata***

179 We reasoned that TFs involved in *CTA1* induction during phosphate starvation must be key to
180 the ASR. Four TFs were implicated in *CTA1*'s induction in *C. glabrata* under H_2O_2 stress, i.e.,
181 Yap1, Skn7, Msn2 and Msn4 (Cuéllar-Cruz *et al.* 2008). To determine which one(s) are
182 responsible for *CTA1* induction under phosphate starvation, we deleted each TF and measured
183 Cta1-GFP induction. We found no effect of *yap1*Δ or *msn2*Δ, while *msn4*Δ and *skn7*Δ both
184 exhibited decreased Cta1 induction during phosphate starvation (Fig. 4A). A double mutant
185 *msn4*Δ *skn7*Δ exhibited more significant reductions in Cta1-GFP levels than either TFΔ alone,
186 suggesting that both Msn4 and Skn7 were required for *CTA1* induction (Fig. 4A). Notably, since
187 Cta1-GFP was still induced in the *msn4*Δ *skn7*Δ strain, additional TFs must be involved. We
188 also noticed that *msn4*Δ and *skn7*Δ affected both the induction and also the basal level of Cta1-
189 GFP before the onset of the starvation (0 min, Fig. 4A). Further analyses showed that except for
190 *msn2*Δ, the other three TF mutants all caused a significant decrease in Cta1 basal levels (Fig.
191 S5A, Bonferroni corrected $P < 0.05$). After normalizing the levels of each strain to the respective
192 0-min level, we confirmed that *msn4*Δ, *skn7*Δ and *msn4*Δ*skn7*Δ showed significant decreases in
193 Cta1 induction under phosphate starvation (Fig. S5B, Bonferroni corrected $P < 0.05$).
194 We also measured Cta1 induction during H_2O_2 treatment and confirmed that both Yap1
195 and Skn7 were required, while *msn4*Δ resulted in a slight decrease in induction and *msn2*Δ had

196 no measurable effect under the H_2O_2 concentration tested (Fig. S5C). This showed that the
197 induction of the same effector gene, i.e., *CTA1*, depended on different TF combinations under
198 different stresses, a result consistent with previous findings in *S. cerevisiae* (Gasch *et al.* 2000).
199 To determine if Msn4 and Skn7 directly regulate *CTA1* under phosphate starvation, we
200 first predicted their binding sites in the promoter of *CTA1* (Fig. 4B). This allowed us to construct
201 a series of promoter mutants, including two internal deletions (200 bp) removing the predicted
202 Msn4 or Skn7 binding sites, as well as point mutations predicted to abrogate Msn4 and Skn7
203 binding (Fig. 4B). For both TFs, we found that all promoter mutants exhibited reduced Cta1-GFP
204 levels similar to the TF deletion strain, with the 200 bp deletion mutants showing the most
205 severe phenotypes (Fig. 4C, D). These results strongly suggest that Msn4 and Skn7 directly
206 regulate *CTA1* during phosphate starvation. In summary, we found that Msn4 and Skn7, along
207 with unidentified TFs, jointly regulate *CTA1* induction in *C. glabrata* under phosphate starvation,
208 while Yap1 and Skn7 were the main TFs responsible for its induction under H_2O_2 stress.

209 **Msn4 translocates into the nucleus upon phosphate starvation in *C. glabrata***

210 Since Msn4 was strongly induced in *C. glabrata* but not in *S. cerevisiae* (Fig. 2F) and several
211 OSR genes induced in *C. glabrata* during phosphate starvation are Msn2/Msn4 targets in *S.*
212 *cerevisiae* (Martínez-Pastor *et al.* 1996; Moskvina *et al.* 1998; Hasan *et al.* 2002), we decided to
213 further investigate the divergence in Msn4's behavior under phosphate starvation. The activity of
214 Msn4 and its paralog Msn2 are partially regulated via nuclear translocation in both *C. glabrata*
215 and *S. cerevisiae* (Görner *et al.* 1998; Cuéllar-Cruz *et al.* 2008; Roetzer *et al.* 2008; Boisnard *et*
216 *al.* 2009). Based on this, we hypothesized that *C. glabrata* Msn4 (CgMsn4), but not its ortholog
217 in *S. cerevisiae* (ScMsn4), translocates into the nucleus upon phosphate starvation. Using GFP-
218 tagged Msn4 and fluorescent microscopy, we found that phosphate starvation led to 47% of the
219 *C. glabrata* cells to have nuclear localized Msn4 ($Msn4^{nuc}$), compared with < 4% in *S. cerevisiae*
220 (Fig. 5, Bonferroni corrected $P < 0.01$). By contrast, glucose starvation led to a similar level of
221 $Msn4^{nuc}$ in both species (Fig. 5, 76% in *C. glabrata* vs 73% in *S. cerevisiae*, raw $P = 0.7$). No
222 significant difference was observed between species under the no-stress condition (raw $P = 1$).
223 These results further support CgMsn4 as one of the TFs mediating the phosphate starvation
224 induced ASR in *C. glabrata* and that divergence in how Msn4 responds to phosphate starvation
225 is a major contributor to the species divergence in ASR. In contrast, we found that the paralog
226 Msn2 translocated into the nucleus in a comparable fraction of cells in the two species under
227 phosphate starvation: 52% in *C. glabrata* and 54% in *S. cerevisiae* (Fig. S6, $P = 0.8$). Combined
228 with the lack of effect of *msn2*Δ on Cta1 induction, we conclude that Msn2 is not involved in the
229 ASR and doesn't contribute to its divergence.

230 **The Greatwall kinase, Rim15, is an important signaling component in the ASR network**

231 Given Msn4's role in the phosphate starvation-induced ASR in *C. glabrata* (Fig. 4, 5), we used it
232 as a bait to identify upstream signaling components in the ASR network. In *S. cerevisiae*, a key
233 regulator of Msn2/Msn4 activity is the Greatwall kinase, Rim15 (Lee *et al.* 2013; Plank 2022).
234 Rim15 itself is regulated by multiple nutrient and stress-sensing kinases, e.g., TORC1, PKA and
235 Pho80/85, making it a central point for integrating nutrient and stress signals (Pedruzzi *et al.*
236 2003; Swinnen *et al.* 2006). We hypothesize that Rim15 regulates the nuclear localization of
237 Msn4 during the primary stress in *C. glabrata* (Fig. 6A). To test this, we compared the nuclear

238 localization of CgMsn4-GFP in the wild type and *rim15*Δ backgrounds. We found that ~68% of
239 the wild type cells had nuclear-localized CgMsn4 during phosphate starvation, compared with
240 only 22% in the *rim15*Δ background (Fig. 6B, $P = 2*10^{-9}$). By contrast, both strain backgrounds
241 showed a low fraction of cells with $CgMsn4^{nuc}$ under high phosphate conditions (Fig. 6B, P =
242 0.2). Next, we asked if Rim15 is required for *CTA1* induction. We found that *rim15*Δ reduced
243 Cta1-GFP induction to a similar level as *msn4*Δ, supporting its role as a regulator of the ASR
244 (Fig. 6C). *msn4*Δ *rim15*Δ had a more severe effect than either deletion alone, suggesting
245 additional players besides the Rim15-Msn4 pathway (Fig. 6C). Lastly, to assess the role of
246 Rim15 in the phosphate starvation-induced ASR, we performed quantitative CFU assays to
247 compare the wild type and *rim15*Δ strains at a comparable strength of H_2O_2 (Fig. 6D). While
248 there is a significant ASR effect in both strains (both P = 0.008), the ASR effect is weaker in
249 *rim15*Δ cells (mean ASR-score = 3.45 for *rim15*Δ, 95% CI = [2.54, 4.33]; mean ASR-score =
250 6.29 for the WT, 95% CI = [4.58, 8.53], Wilcoxon signed-rank test between genotypes, one-
251 sided P = 0.02). Taken together, these results strongly suggest that Rim15 is a crucial signaling
252 component for the phosphate starvation-induced ASR in *C. glabrata*.

253 **Target-Of-Rapamycin Complex 1 (TORC1) is strongly inhibited by phosphate starvation**
254 **in *C. glabrata* but not in *S. cerevisiae***

255 In *S. cerevisiae*, Msn2 and Msn4's nuclear translocation is regulated by both the Target-of-
256 Rapamycin Complex 1 (TORC1) and Protein Kinase A (PKA) pathways (Görner *et al.* 1998;
257 Beck and Hall 1999; Plank 2022). In *S. cerevisiae* TORC1 has a slow and weak response to
258 phosphate limitation (Urban *et al.* 2007). In the distantly related yeast pathogen *C. albicans*,
259 TORC1 was shown to respond rapidly to phosphate availability (Liu *et al.* 2017). We therefore
260 hypothesized that TORC1 is more strongly and quickly inhibited by phosphate starvation in *C.*
261 *glabrata* than in *S. cerevisiae*, contributing to the Msn4-mediated stress response and ASR. To
262 test this, we used the phosphorylation of ribosomal protein S6 (Rps6) as a conserved readout of
263 TORC1 activity (Magnuson *et al.* 2012; González *et al.* 2015; Liu *et al.* 2017). We found 60
264 minutes of phosphate starvation did not affect the total level of Rps6 but markedly reduced the
265 abundance of phosphorylated Rps6 (P-Rps6) in *C. glabrata* (Bonferroni-corrected P = 0.06, Fig.
266 7A, B). The same treatment, however, did not affect the proportion of P-Rps6 in *S. cerevisiae* (P
267 = 1). By contrast, nitrogen starvation rapidly inhibited phosphorylation of Rps6 in both species
268 (P = 0.06 and 0.07). These results confirmed that inhibition of TORC1 by nitrogen starvation is
269 conserved between the two species while only in *C. glabrata* is TORC1 strongly inhibited by
270 phosphate starvation at 60 minutes, consistent with their distinct ASR phenotypes (Fig. 1). To
271 determine which of the two species represents the ancestral state, we performed the same
272 experiment in two outgroup species, *K. lactis* and *L. walti*, which diverged from *S. cerevisiae*
273 and *C. glabrata* approximately 120 million years ago (Shen *et al.* 2018). We found that both
274 outgroups exhibited intermediate phenotypes with respect to TORC1 inhibition by phosphate
275 starvation at 60 minutes, while in all four species, TORC1 was rapidly inhibited by nitrogen
276 starvation (Fig. S7). This suggests that the link between phosphate and TORC1 is ancestral, but
277 the strength of the connection is more evolutionarily labile than nitrogen starvation and TORC1.

278 **Inhibition of TORC1 leads to Msn4 nuclear localization, *CTA1* induction and confers mild**
279 **ASR in *C. glabrata***

280 To determine if TORC1 inhibition by phosphate starvation has the potential to contribute to the
281 ASR, we used rapamycin to inhibit TORC1 and monitored Msn4^{nuc}, Cta1-GFP induction and the
282 ASR effect. We found that TORC1-inhibition induces Msn4^{nuc} in both species, with a stronger
283 effect in *C. glabrata*. Specifically, exposure to 500 ng/mL of rapamycin for 45 minutes led to
284 71.8% (79/110) of *C. glabrata* cells and 14.5% (19/131) of *S. cerevisiae* cells to show Msn4^{nuc}.
285 Both were significantly higher compared with the mock-treated group (1.8% in *C. glabrata* and
286 1.2% in *S. cerevisiae*, FET $P < 0.001$ in both). Next, we followed Cta1-GFP induction in *C.*
287 *glabrata* exposed to rapamycin and found a dose-dependent response except for the highest
288 dose, which resulted in a lower induction than the next dose (Fig. 7C). Lastly, we found 125
289 ng/mL rapamycin treatment for 45 minutes modestly but significantly enhanced the survival of
290 *C. glabrata* after a secondary H_2O_2 stress (Fig. 7E, mean ASR-score = 1.79, 95% CI [1.35,
291 2.28], $P = 0.016$). The same rapamycin dose resulted in a similar increase in survival in *S.*
292 *cerevisiae* (mean ASR-score = 1.81, 95% CI [1.21, 2.47], $P = 0.063$) (Fig. 7E). We conclude that
293 TORC1 inhibition has the potential to induce acquired resistance for H_2O_2 in both species. This
294 implies that divergence of the ASR occurred through TORC1's differential response to -Pi.

295 **TORC1 proximal effector, Sch9, contributes to phosphate starvation-induced ASR, while**
296 **a downstream output of the Tap42-PP2A branch is minimally affected**

297 The AGC kinase Sch9 is directly phosphorylated and regulated by TORC1 (Urban *et al.* 2007).
298 In turn, Sch9 regulates multiple downstream processes, including repressing stress responses
299 by inhibiting Rim15 via phosphorylation, which prevents the latter from activating Msn4 (Wanke
300 *et al.* 2005, 2008). To determine if Sch9 negatively regulate the ASR, we created a TORC1
301 phosphomimetic mutant of CgSch9 predicted to be constitutively active with respect to TORC1
302 signaling (Urban *et al.* 2007) (Fig. S8). This mutant showed reduced Cta1-GFP induction during
303 phosphate starvation (Fig. 7D). Moreover, a quantitative CFU assay failed to detect ASR in this
304 mutant (Fig. 7F, $P = 0.69$), further supporting TORC1's role in the ASR (Fig. 7G).
305 Since TORC1 coordinates multiple cellular processes, we asked if phosphate starvation
306 had limited or broad effects on TORC1's downstream branches (Loewith and Hall 2011). This is
307 important because to achieve optimal growth, TORC1 needs to differentially activate or repress
308 its downstream outputs in a condition-specific manner (Hughes Hallett *et al.* 2014). Therefore,
309 the question is whether evolution can wire an input like phosphate to specific outputs without
310 impacting other branches? To answer this, we monitored the Nitrogen Catabolism Repression
311 (NCR) regulon, because it is primarily controlled by Tap42-PP2A rather than by Sch9, and is
312 differentially induced under nitrogen starvation vs glucose starvation or several stresses in *S.*
313 *cerevisiae* (Hughes Hallett *et al.* 2014). Using an established *DAL80pr*-GFP reporter (Neklesa
314 and Davis 2009), we found that nitrogen starvation strongly induced NCR-sensitive genes, but
315 phosphate starvation had minimal effects in both *S. cerevisiae* and *C. glabrata* (Fig. S9). This
316 suggests that evolution can wire an input such as phosphate limitation to a specific TORC1
317 output, i.e., stress response, without strongly impacting other outputs.

318 **Discussion**

319 Acquired stress resistance (ASR) is suggested to be an adaptive anticipatory response and
320 therefore expected to evolve between species. However, both the genetic basis of ASR and its

evolution remain poorly characterized. In this study, we discovered a divergent ASR phenotype between two related yeasts: in the opportunistic yeast pathogen, *C. glabrata*, a short, non-lethal phosphate starvation provides a strong protective effect for a severe H_2O_2 stress, while in the baker's yeast, *S. cerevisiae*, the same treatment has little to no effect (Fig. 1). We identified a core subnetwork behind the ASR in *C. glabrata*, where phosphate starvation not only induces the canonical phosphate starvation (PHO) response via the TF Pho4, but also induces >15 oxidative stress response (OSR) genes, mediated by two TFs known to be involved in the canonical OSR, Msn4 and Skn7 (Fig. 2, 8A). Divergence in ASR between the two species was explained in part by the differences in nuclear translocation of Msn4 in response to phosphate limitation. Remarkably, the central regulator TORC1 showed differential sensitivity to phosphate in the two species while being similarly affected by nitrogen starvation (Fig. 7), implicating it as a key point of divergence behind ASR evolution, and showing how a conserved, multifunctional complex can be evolutionarily tuned.

We showed that the divergence in the ASR for H_2O_2 between the two species is specific to phosphate – two other primary stresses tested, glucose starvation and heat shock, can elicit a protective effect in both species (Fig. S2). Why phosphate? Several lines of evidence suggest that phosphate and genes involved in the PHO response are relevant in the host environment, including impacting virulence in several infection models and affecting sensitivity to ROS (Ikeh *et al.* 2017; Köhler *et al.* 2020). Moreover, while studies on the phagosome environment mainly focused on nutrients such as glucose, a recent transcriptomic study showed that PHO genes, such as the high affinity transporter *PHO84* and the secreted phosphatases *PMU2* were both highly upregulated within 2 hours of *C. glabrata* being engulfed by human macrophages (Fig. S1) (Rai *et al.* 2021). Conversely, we found that many genes induced and known to be important for survival inside the macrophage were also induced during phosphate starvation in *C. glabrata*, including autophagy, TCA cycle, amino acid biosynthesis and iron homeostasis genes (Fig. S10). This suggests that phosphate limitation is a physiologically relevant stress in the host and may serve as a stimulus to induce ASR for more severe stresses.

In *S. cerevisiae*, chronic phosphate starvation is known to induce cell-cycle arrest and is associated with increased resistance to stress including H_2O_2 (Gresham *et al.* 2011; Petti *et al.* 2011; Carter-O'Connell *et al.* 2012; Ebrahimi *et al.* 2021; Garg *et al.* 2023). Could the phosphate starvation-induced ASR represent a physiological response to starvation? We believe not, due to several distinctions between the ASR after a short phosphate starvation (<2hr) and the effect of chronic starvation (> 5 hrs) of phosphate. First, chronic phosphate starvation leads to cell-cycle arrest after ~10 hrs (Saldanha *et al.* 2004), while during the short phosphate starvation, cells from both species continue to divide up until 105 minutes, with a similar fraction of unbudded cells between species (Fig. S11). Second, chronic starvation of natural nutrients, like phosphate and sulfate, was associated with an expansive transcriptional change that was largely independent of the limiting nutrient (Saldanha *et al.* 2004). This is in contrast to the more specific and restricted response in the short-term phosphate limitation (Ogawa *et al.* 2000; Zhou and O'Shea 2011; He *et al.* 2017). The catalase gene *CTA1*, for example, was not induced during chronic starvation in *S. cerevisiae* (Petti *et al.* 2011). Lastly, we showed that *cta1*Δ didn't affect the survival of *C. glabrata* under phosphate starvation, suggesting its induction primarily

363 benefited cells' survival during the secondary stress (Fig. S4). Thus, we believe the induction of
364 oxidative stress response genes in *C. glabrata* is not part of a general starvation response but
365 likely represents an anticipatory stress response.
366 A major gap in our knowledge is how ASR phenotypes and the underlying networks
367 evolve. For example, does ASR involve the same effector and regulator genes in the canonical
368 response to the secondary stress itself? We found that phosphate starvation-induced ASR in *C.*
369 *glabrata* reused some of the same TFs and effector genes belonging to the canonical OSR but
370 differed in the TF combinatorial grammar in regulating effector genes such as *CTA1*, resulting in
371 distinct induction kinetics (Fig. 3, 8B). Such condition-specific regulation is consistent with
372 findings in *S. cerevisiae*, where shared transcriptional changes across various stresses were
373 found to depend on distinct TF combinations (Gasch *et al.* 2000). We argue that this facilitates
374 evolution by allowing mutations to modify the expression pattern of a gene in one context with
375 little or no impact under another, thereby reducing the pleiotropic effects. Another intriguing
376 finding is that the paralogous TFs, Msn2 and Msn4, showed divergent functions in ASR and
377 H_2O_2 stress between species. In contrast to *S. cerevisiae*, where Msn2 plays a more important
378 role and the two paralogs' functions largely overlap (Berry and Gasch 2008; AkhavanAghdam *et*
379 *al.* 2016; Chapal *et al.* 2019; Wu *et al.* 2021), in *C. glabrata* Msn2 was dispensable for the
380 induction of *CTA1* both during phosphate starvation and H_2O_2 stress while Msn4 played an
381 important role (Fig. 4, 5, S5). We speculate that the maintenance and evolution of TF paralogs
382 is an important source for ASR and, more generally, stress response evolution.
383 Lastly, given the central role and conservation of TORC1 across species, we were
384 surprised to find that its response to phosphate differed significantly, likely directly contributing
385 to the ASR divergence. What's intriguing is that not all nutrient input diverged between the two
386 species: nitrogen starvation strongly suppressed TORC1 in both species as well as two
387 outgroups we tested (Fig. 7, S7). One clue to how a central regulator like TORC1 can evolve
388 without having pleiotropic effects came from our finding that phosphate starvation very weakly
389 affected the branch of TORC1 associated with nitrogen catabolism, which is strongly induced by
390 nitrogen starvation (Fig. S9). Contrasting phosphate with nitrogen starvation, we can gain an
391 important insight into TORC1's evolution: with multiple inputs and output branches, since each
392 of the inputs can be wired differently to the output branches, this allows evolution to rewire
393 specific inputs with specific outputs and potentially avoids the pleiotropic effects that could
394 otherwise jeopardize evolution (Fig. 8C).

395 **Materials and Methods**

396 **Experimental reproducibility and data availability**

397 Each experiments was repeated at least two times, with most experiments repeated three or
398 more times with >2 biological replicates each. Data analysis and visualization were performed in
399 R v4.2. Raw data, R markdown files, and output files are available at https://github.com/binhe-
400 lab/E036-ASR-H2O2. This repository will be version controlled by Zenodo upon publication.

401 **Yeast media and growth conditions**

402 Yeast cells were grown in Yeast extract-Peptone Dextrose (YPD) or synthetic complete (SC,
403 using Yeast Nitrogen Base without amino acids, Sigma Y0626) medium. Unless specified, all

404 stress treatments were performed with mid-log phase cells. Briefly, cells were grown overnight
405 in rich media, diluted in the morning to OD_{600} = 0.2 and grown to OD_{600} ~ 1. To apply treatments,
406 cells were collected by centrifugation at 3,000g for 5 minutes, washed 2-3 times with water and
407 released into the treatment media. Rapamycin (RPI, R64500) was added into the medium at the
408 indicated concentrations. Nitrogen starvation medium was made using the Yeast Nitrogen Base
409 without amino acids and without ammonium sulfate (Sigma, Y1251). Glucose starvation medium
410 was made by omitting the glucose in the SC medium. Phosphate starvation medium was made
411 using Yeast Nitrogen Base with ammonium sulfate, without phosphates, without sodium chloride
412 (MP Biomedicals, 114027812) and supplemented to a final concentration of 2% glucose, 1.5
413 mg/ml potassium chloride, 0.1 mg/ml sodium chloride and amino acids, as described previously
414 (He *et al.* 2017). Phosphate concentration in the medium was measured using a Malachite
415 Green Phosphate Assay kit (Sigma, MAK307). To apply H_2O_2 stress, H_2O_2 stock solution (30%
416 w/w, Sigma H1009) was diluted into SC medium to the indicated concentrations immediately
417 before the experiment.

418 **Generating yeast strains and plasmids**

419 Genetic transformation of both *S. cerevisiae* and *C. glabrata* was performed using the LiAc
420 method as described in (Gietz and Schiestl 2007). *C. glabrata* knockout strains were generated
421 with auxotrophic markers *HIS3* and *URA3* and the nourseothricin resistant gene Nat. ~500 bp of
422 flanking homology sequences were added to either a deletion cassette or a knock-in construct
423 using overlap PCR. Transformants were confirmed by colony PCR on both sides of the gene.
424 To construct *CTA1* promoter mutants, a URA3 marker was used to replace the endogenous
425 promoter, after which the mutant allele constructed by PCR mutagenesis was used as the repair
426 template to swap out the URA3 and selecting with 5-fluoroorotic acid (5-FOA) (GoldBio, F-320).
427 To construct the Msn2 and Msn4-GFP expression plasmids and the *ScDAL80*-GFP plasmid, the
428 pCU-PDC1-GFP and SV195 plasmids were used as backbones. Gibson cloning was performed
429 according to the protocols for the Gibson Assembly kit (NEB, E5520). To construct the Sch9-3E-
430 Nat and the matching Sch9-WT-Nat control strains at the endogenous site, the Sch9-3E and
431 Sch9-WT fragments were joined with the Nat cassette via overlap PCR. The end products had
432 ~200bp of flanking homology sequences on both sides. Positive transformants were selected on
433 YPD+Nat plates and validated by genomic PCR. Yeast strains and plasmids used in this study
434 are listed in Table 1 and Table 2, respectively.

435 **Spotting and Colony Forming Units (CFU) assays**

436 A semi-quantitative spotting assay or a quantitative Colony Forming Unit (CFU) assay was used
437 to measure the survival rate after a treatment. For the spotting assay, the treated cells were 10x
438 serially diluted in ddH_2O. 5 µl of each dilution was spotted onto an SC plate and allowed to dry
439 before the plate was incubated at 30C for 16-36 hours. An image was taken at the end of the
440 incubation using a homemade imaging hood fitted with an iPad Air. For the CFU assay, post-
441 treatment cells were diluted 100 to 1,000-fold and plated on an SC plate. The dilution was
442 chosen to produce roughly 10-500 colonies per plate. The plates were incubated for 48 hours
443 and CFU was manually counted using a lab counter (Fisher Scientific).

444 **Calibrating H_2O_2 concentrations**

445 To apply an equivalent strength of H_2O_2 treatment to species and genotypes with different basal
446 survival rates, we measured the cell survival rates after treatment with different concentrations
447 of H_2O_2. As an example, we exposed *S. cerevisiae* cells to a series of H_2O_2 concentrations from
448 0mM to 10mM, with 2mM steps. Similarly, we exposed *C. glabrata* cells H_2O_2 concentrations
449 from 0mM to 100mM with 20mM steps. To quantitatively estimate the survival rate, CFU assays
450 were performed after 2 hours of treatment to estimate the survival rate. Concentrations resulting
451 in similar survival rates across species (or genotypes) were chosen as the condition for the
452 secondary stress in the ASR experiment.

453 **Acquired stress resistance (ASR) assay**

454 Mid-log phase cells were transferred to the SC medium (mock) or the 0 mM Pi SC medium
455 (phosphate starvation) or other indicated stress media for the primary stress. After 45 minutes
456 (or as indicated) of incubation with shaking at 30 C, cells were collected by centrifugation,
457 resuspended at OD_{600} = 0.2 in the secondary stress treatment media for 2 hours. After the
458 secondary stress, either a spotting assay or a CFU assay was performed. CFU multiplied by the
459 fold dilution was used to calculate r (MO/MM), r (PO/PM)' and the ASR-score (r'/r). At least
460 three biological replicate experiments were performed.

461 **RNA-seq profiling for *C. glabrata* under phosphate starvation**

462 *C. glabrata* wild type cells were grown in SC overnight, diluted into fresh SC the next morning to
463 OD_{600} = 0.1, grown for another 2-3 hours until the culture reached mid-log phase (OD_{600}~0.6). At
464 this point, two biological replicates of pre-starvation samples were collected using a cold
465 methanol quenching method (Pieterse *et al.* 2006; Zhou and O'Shea 2011). Briefly, 5 mL of
466 culture was added directly into 7.5 mL of pre-chilled methanol (−50°C) and incubated in an
467 ethanol-dry ice bath at that temperature for at least 20 min. The remaining culture was collected
468 by filtration, washed with equal volume of pre-warmed no phosphate SC media and then
469 released into the pre-warmed no phosphate SC. After 1 hour incubation with shaking at 30 C,
470 three biological replicates of the starved samples were collected in the same way as above.
471 When all samples were in the ethanol-dry ice bath for > 20 minutes, cells were collected by
472 centrifugation and quickly washed with ice-cold water to remove the methanol and resuspended
473 in RNAlater solution (Qiagen, 76104) for at least 2 hours. Cells were centrifuged to remove the
474 RNAlater, flash-frozen in liquid nitrogen and stored at -80 C until RNA-extraction. For each
475 sample, ~$5x10^7$ cells were collected and total RNA was extracted using a MasterPure Yeast
476 RNA purification kit (Biosearch Technologies, MPY03100) following the manufacturer's protocol.
477 RNA-seq libraries were prepared with the TruSeq RNA Library Preparation Kit v2 (Illumina) with
478 the mRNA purification option. The resulting libraries were sequenced on an Illumina HiSeq
479 4000, which produced on average 10 million 50 bp single end reads for each sample.

480 **Comparing the transcriptional response to phosphate starvation between *C. glabrata* and**
481 ***S. cerevisiae***

482 The RNA-seq raw reads were mapped to the *C. glabrata* genome downloaded from the Candida
483 Genome Database (CGD, RRID:SCR_002036, version s02-m02-r09), using Bowtie v1.1.1
484 (RRID:SCR_005476) with the option '-m 1 --best –strata' (Langmead *et al.* 2009). The resulting
485 SAM files were sorted using Samtools v1.2 (RRID:SCR_002105) (Li *et al.* 2009) and the

486 number of reads per transcript was counted using Bedtools2 (RRID:SCR_006646) (Quinlan and
487 Hall 2010), with the option 'bedtools coverage -a BAM_file -b genome_annotation.bed -S -s
488 sorted -g Chrom.length`. Gene features for *C. glabrata* were downloaded from CGD, version
489 s02-m07-r04. The count matrix was filtered to remove lowly expressed genes (335 genes with
490 <1 read per sample on average). Next, we used the trimmed mean of M-values ('TMM') method
491 in the EdgeR (RRID:SCR_012802) package to calculate the normalization factors for scaling the
492 raw library sizes (Robinson *et al.* 2010), and applied voom transformation (Law *et al.* 2014) to
493 remove the mean-variance relationship on the log2 transformed count data. A log2 fold change
494 was calculated for each gene by subtracting the mean of the pre-starvation samples from each
495 of the 1-hr starvation sample values. For *S. cerevisiae*, the microarray data from (Zhou and
496 O'Shea 2011) was downloaded from the GEO database (RRID:SCR_005012). Within the series
497 GSE23580, three samples corresponding to the three biological replicates comparing the 1 hour
498 phosphate starved sample to a mock-treated sample were extracted (GSM578408, 578424,
499 578440). The log2 ratios were already background-subtracted, normalized, and were used
500 directly for comparisons. To compare orthologous gene expression, we first curated a list of
501 oxidative stress response genes based on the literature (Table S1) (Lee *et al.* 1999; Hasan *et*
502 *al.* 2002). To identify their homologs in *C. glabrata*, we downloaded the orthology and best-hit
503 mapping between the two species from CGD. The best-hit mapping was based on less stringent
504 criteria and only used when an orthology mapping was not available. The resulting table of gene
505 expression log2 fold changes is available in Table S2.

506 ***CTA1* induction by quantitative real-time PCR (qRT-PCR)**

507 *C. glabrata* cells were mock-treated or treated with phosphate starvation or 1.5 mM H_2O_2 for 45
508 minutes. ~2-4x10^7 cells were harvested by centrifugation, snap-frozen in liquid nitrogen and
509 stored in -80 until RNA extraction. Two biological replicates were collected per condition. RNA
510 was extracted using a MasterPure Yeast RNA purification kit (Biosearch Technologies,
511 MPY03100). cDNA was synthesized using SuperScript™ III First-Strand Synthesis System
512 (Invitrogen, 18080051) and treated with RNase A (ThermoFisher, EN0531). We used the
513 LightCycler® 480 SYBR Green I Master (Roche, 04707516001) and qRT-PCR was performed
514 on a Roche LC480 instrument. Three technical replicates were performed for each sample. The
515 PCR program was 95°C for 5 minutes, followed by 45 cycles of 95°C for 10 seconds, 60°C for
516 20 seconds, and 72°C for 20 seconds. Data analysis was done using the instrument software,
517 including automatic baseline subtraction and C_T value quantifications. *ACT1* was used as a
518 reference gene and its C_T values were subtracted from those of *CTA1*. We then subtracted the
519 mean of the ΔC_T for the mock-treated samples from the technical replicates for the phosphate
520 starvation and H_2O_2-treated ones to obtain $\Delta\Delta C_T$, which were used for downstream analyses.

521 **Cta1-GFP time course by flow cytometry**

522 Cells were grown to mid-log phase in SC medium in 96 deep-well plates (VWR, 82051). After
523 washing with ddH_2O twice and spinning down at 3,000g for 5 minutes, cells were resuspended
524 in 0mM Pi SC medium, H_2O_2-containing SC medium and SC medium (7.5mM Pi), incubated at
525 30°C shaking at 200 rpm for 4 hrs. At the indicated time points, an aliquot of cell culture (40 -
526 50uL) was drawn and diluted into ddH_2O (360uL - 400uL) for flow cytometry on an Attune NxT

527 instrument fitted with an autosampler (Thermo Fisher). For each sample, 30,000 events were
528 recorded, non-cell events and doublets were removed based on FSC-H and FSC-W. Median
529 fluorescence intensity (MFI) was used for Cta1-GFP protein expression analysis.

530 **Binding site prediction for *CTA1* promoter**

531 To predict the binding sites (BS) for Skn7 and Msn4 in the *CgCTA1* promoter, we first retrieved
532 the 1000 bp DNA upstream of the start codon for the *CTA1* gene in the *C. glabrata* CBS138
533 genome (CGD, version s02-m02-r09). We then scanned this sequence with the expert curated
534 motifs for Skn7 and Msn4 from the Yetfasco (yetfasco.ccbr.utoronto.ca) database. To perform
535 the scanning, we first selected the two motifs for Skn7 and single expert curated motif for Msn4,
536 "added them to the cart", and used the "scan using cart" function. We adopted the default 75%
537 minimum percent of maximum score cutoff, and set the background percent A/T to 0.3, which
538 was based on the mean GC% in 1000 bp upstream sequences in the *C. glabrata* genome
539 calculated in-house. The motifs and prediction results were available in Supplementary Text S1.

540 **Fluorescent microscopy for Msn4 and Msn2 nuclear localization**

541 *C. glabrata* cells were transformed with the indicated plasmids and grown on SC Ura- plates for
542 selection. Transformed cells were then grown and maintained in SC Ura- liquid medium prior to
543 the experiments. *C. glabrata* cells were grown to mid-log phase in SC Ura- medium and treated
544 with SC complete, glucose starvation, or 0mM Pi SC media for 30 mins. Subsequently, 4',6-
545 diamidino-2-phenylindole (DAPI, Sigma, D9542) was diluted in the respective medium and
546 added to the cultures at a final concentration of 10 ng/ml. Cells were incubated with DAPI in the
547 dark for 15 minutes before DAPI was removed and cells were washed twice with ddH_2O. Finally,
548 cells were re-resuspended in the treatment medium. Fluorescent imaging was performed on a
549 Leica SP8 confocal imaging system (Carver Center for Imaging, the University of Iowa). A 488
550 nm laser was used for yeGFP excitation and 495-585 nm for emission; a 405 nm laser was
551 used for DAPI excitation and 430-550 nm for emission. In *S. cerevisiae*, Msn2-mCherry and
552 Msn4-mCitrine cells were prepared as described above excluding the DAPI staining. For Msn4-
553 mCitrine, 488 nm was used for excitation and 501-547 nm for emission; for mCherry, 552 nm
554 was used for excitation and 570-649 nm for emission; for visualizing the nucleus with the
555 Nhp6a-iRFP marker, a 638 nm laser was used for excitation and 648-790 nm for emission.

556 **Total and P-Rps6 Western Blot**

557 Mid-log phase cells were subjected to either mock or starvation treatments in parallel. Cell lysis
558 buffer (0.1M NaOH, 0.05M EDTA, 2% SDS, 2% β-mercaptoethanol) and loading buffer (0.25M
559 Tris-HCL pH6.8, 50% Glycerol, 0.05% bromophenol blue) were prepared and protein extraction
560 was performed as described in (von der Haar 2007). Cell lysates were separated by SDS-PAGE
561 at 200 volts for 40 minutes, transferred onto nitrocellulose membranes (Bio-Rad, 1662807), and
562 stained with a total protein stain (Li-COR, 926-11015), which we used for normalization in place
563 of a loading control, as recommended by Li-COR. The membranes were blocked with 3% BSA
564 (RPI, A30075) at room temperature for 1 hr. Two blots for the same samples were probed with
565 either anti-phospho (Ser/Thr) Akt substrate rabbit polyclonal antibody (RRID:AB_330302, Cell
566 Signaling Technology # 9611) or Anti-RPS6 rabbit antibody (RRID:AB_945319, Abcam

567 ab40820) to detect the phosphorylated Rps6 (P-Rps6) and total S6, respectively. After washing,
568 the blots were incubated with a secondary antibody (RRID:AB_621843, LI-COR, 926-32211)
569 and were imaged on a Li-COR Odyssey scanner (Carver Center for Genomics, the University of
570 Iowa). The intensity of the total protein stain and Western Blot were quantified using Li-COR
571 onboard software. Background was subtracted on the Western Blot image using a region next to
572 the lane of interest. The ratio of P-Rps6 to total Rps6 was calculated for each sample.

573 **Assaying cell morphology by light microscopy**

574 To determine the percent of unbudded cells during a phosphate starvation time course, wild
575 type *C. glabrata* and *S. cerevisiae* cells were grown as described above to mid-log phase,
576 collected by centrifugation, washed once with pre-warmed 0 mM Pi media and diluted to $5x10^6$
577 cells/mL in 0 mM Pi media. At 0, 20, 45, 75, 105 and 135 minutes into the time course, an
578 aliquot of cells was taken from each sample, sonicated for 5s to break up any cell clumps,
579 diluted 10-50x and counted on a hemocytometer (Marienfeld, 0640030) under a light
580 microscope. The number of unbudded cells over the total number of cells were recorded by
581 manually examining > 100 cells over four fields of view. The numbers from the four fields of
582 view were summed for downstream analysis.

583 **Statistical analyses and tests**

584 For <u>*quantitative ASR assays*</u> using CFU, the data from each replicate experiment were used to
585 calculate survival rates with or without the primary stress, expressed as $r = CFU_{MO} / CFU_{MM}$ and
586 $r' = CFU_{PO} / CFU_{PM}$. The fold change in survival due to the primary stress, calculated as r/r' and
587 referred to as ASR-score, was calculated for each experiment. We estimated the mean and
588 95% confidence interval for the ASR-score with 1000 bootstraps using the smean.cl.boot()
589 function in the Hmisc package. To assess the statistical significance of the ASR effect, we used
590 the paired r and r' estimates from each replicate and performed either a Wilcoxon signed-rank
591 test if n >= 4, or a paired Student's t-test when n < 4, because the former test has extremely low
592 power at such a small sample size. The one-sided *P*-value, with the alternative hypothesis being
593 r' > r, was reported in the legend and text. For <u>*transcriptomic comparisons*</u>, we performed a t-
594 test for the triplicates of the log2 fold changes for 29 genes in both species. The alternative
595 hypothesis was that the true log2 fold change was greater than 0 (induced under phosphate
596 starvation). The resulting *P*-values were adjusted for multiple comparisons using the Benjamini-
597 Hochberg procedure (FDR). Genes with an FDR < 0.05 and a log2 fold change > 2 were
598 considered significantly induced. For <u>*CTA1 induction by qRT-PCR*</u>, the $\Delta\Delta C_T$ values from the
599 three technical replicates for the phosphate starved, H_2O_2-treated and mock-treated samples
600 were analyzed using a linear model, with the two stress conditions treated as dummy variables
601 and the biological replicate included as a covariate (R: lm(ddCt ~ treatment + strain), where
602 treatment is a factor with levels = {"Mock", "-Pi", "H_2O_2"}). Raw *P*-values for each level were
603 reported. For <u>Cta1-GFP basal and induced levels</u>, a linear model was used to compare the
604 different genotypes and the *P*-values were Bonferroni-corrected (multiplied by 5 mutants). The
605 same linear model approach was applied to the 120-min data after subtracting the 0-min levels
606 for each genotype. For <u>*Msn4 nuclear localization*</u>, cells with nuclear-localized vs cytoplasmic
607 Msn4 were counted under a fluorescent microscope (>100 cells in total per strain x condition). A

608 Fisher's Exact Test (FET) was performed for cells with or without nuclear-localized Msn4 and
609 between species/genotypes. *P*-values were calculated using an exact method. When multiple
610 comparisons were made, a Bonferroni correction was applied unless otherwise noted in the text
611 or legend. For *Western Blot analysis of P-Rps6 / total Rps6*, the samples being compared were
612 run on the same gel for each replicate. Thus, a paired Student's t-test was performed, and a
613 two-sided *P*-values after Bonferroni correction was used to assess the significance of the
614 difference between the treatment conditions.

615 **Acknowledgement**

616 We thank Lan Qing and Chris Koon for kindly providing the PolII ChIP-seq data for PHO gene
617 induction in phagocytosed *C. glabrata*.

618 **Funding**

619 Dr. Bin Z. He is supported by NIH R35GM137831 and a start-up fund provided by the University
620 of Iowa.

621 **Literature Cited**

622 AkhavanAghdam Z., J. Sinha, O. P. Tabbaa, and N. Hao, 2016 Dynamic control of gene
623 regulatory logic by seemingly redundant transcription factors. eLife 5: e18458.
624 https://doi.org/10.7554/eLife.18458

625 Beck T., and M. N. Hall, 1999 The TOR signalling pathway controls nuclear localization of
626 nutrient-regulated transcription factors. Nature 402: 689–692. https://doi.org/10.1038/45287

627 Berry D. B., and A. P. Gasch, 2008 Stress-activated Genomic Expression Changes Serve a
628 Preparative Role for Impending Stress in Yeast. Mol. Biol. Cell 19: 4580–4587.
629 https://doi.org/10.1091/mbc.E07-07-0680

630 Berry D. B., Q. Guan, J. Hose, S. Haroon, M. Gebbia, *et al.*, 2011 Multiple means to the same
631 end: the genetic basis of acquired stress resistance in yeast. PLoS Genet. 7: e1002353.
632 https://doi.org/10.1371/journal.pgen.1002353

633 Boisnard S., G. Lagniel, C. Garmendia-Torres, M. Molin, E. Boy-Marcotte, *et al.*, 2009 H2O2
634 Activates the Nuclear Localization of Msn2 and Maf1 through Thioredoxins in Saccharomyces
635 cerevisiae. Eukaryot. Cell 8: 1429. https://doi.org/10.1128/EC.00106-09

636 Brown A. J. P., D. E. Larcombe, and A. Pradhan, 2020 Thoughts on the evolution of Core
637 Environmental Responses in yeasts. Fungal Biol. 124: 475–481.
638 https://doi.org/10.1016/j.funbio.2020.01.003

639 Brunke S., and B. Hube, 2013 Two unlike cousins: Candida albicans and C. glabrata infection
640 strategies. Cell. Microbiol. 15: 701–708. https://doi.org/10.1111/cmi.12091

641 Carter-O'Connell I., M. T. Peel, D. D. Wykoff, and E. K. O'Shea, 2012 Genome-wide
642 characterization of the phosphate starvation response in Schizosaccharomyces pombe. BMC
643 Genomics 13: 697. https://doi.org/10.1186/1471-2164-13-697

644 Chapal M., S. Mintzer, S. Brodsky, M. Carmi, and N. Barkai, 2019 Resolving noise-control
645 conflict by gene duplication. PLoS Biol. 17: e3000289.
646 https://doi.org/10.1371/journal.pbio.3000289

647 Chen D., W. M. Toone, J. Mata, R. Lyne, G. Burns, *et al.*, 2003 Global transcriptional responses
648 of fission yeast to environmental stress. Mol. Biol. Cell 14: 214–229.
649 https://doi.org/10.1091/mbc.E02-08-0499

650 Cuéllar-Cruz M., M. Briones-Martin-del-Campo, I. Cañas-Villamar, J. Montalvo-Arredondo, L.
651 Riego-Ruiz, *et al.*, 2008 High Resistance to Oxidative Stress in the Fungal Pathogen Candida
652 glabrata Is Mediated by a Single Catalase, Cta1p, and Is Controlled by the Transcription Factors
653 Yap1p, Skn7p, Msn2p, and Msn4p. Eukaryot. Cell 7: 814–825.
654 https://doi.org/10.1128/EC.00011-08

655 Davies K. J. A., 2016 Adaptive homeostasis. Mol. Aspects Med. 49: 1–7.
656 https://doi.org/10.1016/j.mam.2016.04.007

657 Dujon B., D. Sherman, G. Fischer, P. Durrens, S. Casaregola, *et al.*, 2004 Genome evolution in
658 yeasts. Nature 430: 35–44. https://doi.org/10.1038/nature02579

659 Durrant W. E., and X. Dong, 2004 Systemic acquired resistance. Annu. Rev. Phytopathol. 42:
660 185–209. https://doi.org/10.1146/annurev.phyto.42.040803.140421

661 Ebrahimi M., L. Habernig, F. Broeskamp, A. Aufschnaiter, J. Diessl, *et al.*, 2021 Phosphate
662 Restriction Promotes Longevity via Activation of Autophagy and the Multivesicular Body
663 Pathway. Cells 10. https://doi.org/10.3390/cells10113161

664 Fidel P. L., J. A. Vazquez, and J. D. Sobel, 1999 Candida glabrata: Review of Epidemiology,
665 Pathogenesis, and Clinical Disease with Comparison to C. albicans. Clin. Microbiol. Rev. 12:
666 80–96.

667 Garg A., A. M. Sanchez, M. Miele, B. Schwer, and S. Shuman, 2023 Cellular responses to long-
668 term phosphate starvation of fission yeast: Maf1 determines fate choice between quiescence
669 and death associated with aberrant tRNA biogenesis. Nucleic Acids Res. gkad063.
670 https://doi.org/10.1093/nar/gkad063

671 Gasch A. P., P. T. Spellman, C. M. Kao, O. Carmel-Harel, M. B. Eisen, *et al.*, 2000 Genomic
672 expression programs in the response of yeast cells to environmental changes. Mol. Biol. Cell
673 11: 4241–4257.

674 Gietz R. D., and R. H. Schiestl, 2007 High-efficiency yeast transformation using the LiAc/SS
675 carrier DNA/PEG method. Nat. Protoc. 2: 31–34. https://doi.org/10.1038/nprot.2007.13

676 González A., M. Shimobayashi, T. Eisenberg, D. A. Merle, T. Pendl, *et al.*, 2015 TORC1
677 Promotes Phosphorylation of Ribosomal Protein S6 via the AGC Kinase Ypk3 in
678 Saccharomyces cerevisiae. PLOS ONE 10: e0120250.
679 https://doi.org/10.1371/journal.pone.0120250

680 Görner W., E. Durchschlag, M. T. Martinez-Pastor, F. Estruch, G. Ammerer, *et al.*, 1998 Nuclear
681 localization of the C2H2 zinc finger protein Msn2p is regulated by stress and protein kinase A
682 activity. Genes Dev. 12: 586–597. https://doi.org/10.1101/gad.12.4.586

683 Goulev Y., S. Morlot, A. Matifas, B. Huang, M. Molin, *et al.*, 2017 Nonlinear feedback drives
684 homeostatic plasticity in H2O2 stress response. eLife 6: e23971.
685 https://doi.org/10.7554/eLife.23971

686 Gresham D., V. M. Boer, A. Caudy, N. Ziv, N. J. Brandt, *et al.*, 2011 System-level analysis of
687 genes and functions affecting survival during nutrient starvation in Saccharomyces cerevisiae.
688 Genetics 187: 299–317. https://doi.org/10.1534/genetics.110.120766

689 Haar T. von der, 2007 Optimized protein extraction for quantitative proteomics of yeasts. PloS
690 One 2: e1078. https://doi.org/10.1371/journal.pone.0001078

691 Hasan R., C. Leroy, A.-D. Isnard, J. Labarre, E. Boy-Marcotte, *et al.*, 2002 The control of the
692 yeast H2O2 response by the Msn2/4 transcription factors. Mol. Microbiol. 45: 233–241.
693 https://doi.org/10.1046/j.1365-2958.2002.03011.x

694 He B. Z., X. Zhou, and E. K. O'Shea, 2017 Evolution of reduced co-activator dependence led to
695 target expansion of a starvation response pathway. eLife 6. https://doi.org/10.7554/eLife.25157

696 Hecker M., J. Pané-Farré, and U. Völker, 2007 SigB-dependent general stress response in
697 Bacillus subtilis and related gram-positive bacteria. Annu. Rev. Microbiol. 61: 215–236.
698 https://doi.org/10.1146/annurev.micro.61.080706.093445

699 Hughes Hallett J. E., X. Luo, and A. P. Capaldi, 2014 State transitions in the TORC1 signaling
700 pathway and information processing in Saccharomyces cerevisiae. Genetics 198: 773–786.
701 https://doi.org/10.1534/genetics.114.168369

702 Ikeh M. A. C., S. L. Kastora, A. M. Day, C. M. Herrero-de-Dios, E. Tarrant, *et al.*, 2016 Pho4
703 mediates phosphate acquisition in Candida albicans and is vital for stress resistance and metal
704 homeostasis. Mol. Biol. Cell mbc.E16-05-0266. https://doi.org/10.1091/mbc.E16-05-0266

705 Ikeh M., Y. Ahmed, and J. Quinn, 2017 Phosphate Acquisition and Virulence in Human Fungal
706 Pathogens. Microorganisms 5. https://doi.org/10.3390/microorganisms5030048

707 Jamieson D. J., 1998 Oxidative stress responses of the yeast Saccharomyces cerevisiae. Yeast
708 14: 1511–1527. https://doi.org/10.1002/(SICI)1097-0061(199812)14:16<1511::AID-
709 YEA356>3.0.CO;2-S

710 Köhler J. R., M. Acosta-Zaldívar, and W. Qi, 2020 Phosphate in Virulence of Candida albicans
711 and Candida glabrata. J. Fungi Basel Switz. 6: E40. https://doi.org/10.3390/jof6020040

712 Kumar K., F. Askari, M. S. Sahu, and R. Kaur, 2019 Candida glabrata: A Lot More Than Meets
713 the Eye. Microorganisms 7: 39. https://doi.org/10.3390/microorganisms7020039

714 Langmead B., C. Trapnell, M. Pop, and S. L. Salzberg, 2009 Ultrafast and memory-efficient
715 alignment of short DNA sequences to the human genome. Genome Biol. 10: R25.
716 https://doi.org/10.1186/gb-2009-10-3-r25

717 Law C. W., Y. Chen, W. Shi, and G. K. Smyth, 2014 voom: precision weights unlock linear
718 model analysis tools for RNA-seq read counts. Genome Biol. 15: R29.
719 https://doi.org/10.1186/gb-2014-15-2-r29

720 Lee J., C. Godon, G. Lagniel, D. Spector, J. Garin, *et al.*, 1999 Yap1 and Skn7 Control Two
721 Specialized Oxidative Stress Response Regulons in Yeast. J. Biol. Chem. 274: 16040–16046.
722 https://doi.org/10.1074/jbc.274.23.16040

723 Lee P., M. S. Kim, S.-M. Paik, S.-H. Choi, B.-R. Cho, *et al.*, 2013 Rim15-dependent activation of
724 Hsf1 and Msn2/4 transcription factors by direct phosphorylation in Saccharomyces cerevisiae.
725 FEBS Lett. 587: 3648–3655. https://doi.org/10.1016/j.febslet.2013.10.004

Leroi A. M., A. F. Bennett, and R. E. Lenski, 1994 Temperature acclimation and competitive fitness: an experimental test of the beneficial acclimation assumption. Proc. Natl. Acad. Sci. U. S. A. 91: 1917–1921. https://doi.org/10.1073/pnas.91.5.1917

Lev S., K. Kaufman-Francis, D. Desmarini, P. G. Juillard, C. Li, *et al.*, 2017 Pho4 Is Essential for Dissemination of Cryptococcus neoformans to the Host Brain by Promoting Phosphate Uptake and Growth at Alkaline pH. mSphere 2. https://doi.org/10.1128/mSphere.00381-16

Li H., B. Handsaker, A. Wysoker, T. Fennell, J. Ruan, *et al.*, 2009 The Sequence Alignment/Map format and SAMtools. Bioinforma. Oxf. Engl. 25: 2078–2079. https://doi.org/10.1093/bioinformatics/btp352

Liu N.-N., P. R. Flanagan, J. Zeng, N. M. Jani, M. E. Cardenas, *et al.*, 2017 Phosphate is the third nutrient monitored by TOR in Candida albicans and provides a target for fungal-specific indirect TOR inhibition. Proc. Natl. Acad. Sci. 114: 6346–6351. https://doi.org/10.1073/pnas.1617799114

Liu N.-N., P. Uppuluri, A. Broggi, A. Besold, K. Ryman, *et al.*, 2018 Intersection of phosphate transport, oxidative stress and TOR signalling in Candida albicans virulence. PLOS Pathog. 14: e1007076. https://doi.org/10.1371/journal.ppat.1007076

Loewith R., and M. N. Hall, 2011 Target of rapamycin (TOR) in nutrient signaling and growth control. Genetics 189: 1177–1201. https://doi.org/10.1534/genetics.111.133363

Lou Y., and A. E. Yousef, 1997 Adaptation to sublethal environmental stresses protects Listeria monocytogenes against lethal preservation factors. Appl. Environ. Microbiol. 63: 1252–1255. https://doi.org/10.1128/aem.63.4.1252-1255.1997

Lu D., N. Maulik, I. I. Moraru, D. L. Kreutzer, and D. K. Das, 1993 Molecular adaptation of vascular endothelial cells to oxidative stress. Am. J. Physiol. 264: C715-722. https://doi.org/10.1152/ajpcell.1993.264.3.C715

Magnuson B., B. Ekim, and D. C. Fingar, 2012 Regulation and function of ribosomal protein S6 kinase (S6K) within mTOR signalling networks. Biochem. J. 441: 1–21. https://doi.org/10.1042/BJ20110892

Martínez-Pastor M. T., G. Marchler, C. Schüller, A. Marchler-Bauer, H. Ruis, *et al.*, 1996 The Saccharomyces cerevisiae zinc finger proteins Msn2p and Msn4p are required for transcriptional induction through the stress response element (STRE). EMBO J. 15: 2227–2235.

Mason D. A., N. Shulga, S. Undavai, E. Ferrando-May, M. F. Rexach, *et al.*, 2005 Increased nuclear envelope permeability and Pep4p-dependent degradation of nucleoporins during hydrogen peroxide-induced cell death. FEMS Yeast Res. 5: 1237–1251. https://doi.org/10.1016/j.femsyr.2005.07.008

Mitchell A., G. H. Romano, B. Groisman, A. Yona, E. Dekel, *et al.*, 2009 Adaptive prediction of environmental changes by microorganisms. Nature 460: 220–224. https://doi.org/10.1038/nature08112

Moskvina E., C. Schüller, C. T. Maurer, W. H. Mager, and H. Ruis, 1998 A search in the genome of Saccharomyces cerevisiae for genes regulated via stress response elements. Yeast Chichester Engl. 14: 1041–1050. https://doi.org/10.1002/(SICI)1097-0061(199808)14:11<1041::AID-YEA296>3.0.CO;2-4

767 Neklesa T. K., and R. W. Davis, 2009 A Genome-Wide Screen for Regulators of TORC1 in
768 Response to Amino Acid Starvation Reveals a Conserved Npr2/3 Complex. PLOS Genet. 5:
769 e1000515. https://doi.org/10.1371/journal.pgen.1000515

770 Nikolaou E., I. Agrafioti, M. Stumpf, J. Quinn, I. Stansfield, *et al.*, 2009 Phylogenetic diversity of
771 stress signalling pathways in fungi. BMC Evol. Biol. 9: 44. https://doi.org/10.1186/1471-2148-9-
772 44

773 Ogawa N., J. DeRisi, and P. O. Brown, 2000 New Components of a System for Phosphate
774 Accumulation and Polyphosphate Metabolism in Saccharomyces cerevisiae Revealed by
775 Genomic Expression Analysis. Mol. Biol. Cell 11: 4309–4321.

776 Pedruzzi I., F. Dubouloz, E. Cameroni, V. Wanke, J. Roosen, *et al.*, 2003 TOR and PKA
777 signaling pathways converge on the protein kinase Rim15 to control entry into G0. Mol. Cell 12:
778 1607–1613. https://doi.org/10.1016/s1097-2765(03)00485-4

779 Petti A. A., C. A. Crutchfield, J. D. Rabinowitz, and D. Botstein, 2011 Survival of starving yeast
780 is correlated with oxidative stress response and nonrespiratory mitochondrial function. Proc.
781 Natl. Acad. Sci. 108: E1089–E1098. https://doi.org/10.1073/pnas.1101494108

782 Pieterse B., R. H. Jellema, and M. J. van der Werf, 2006 Quenching of microbial samples for
783 increased reliability of microarray data. J. Microbiol. Methods 64: 207–216.
784 https://doi.org/10.1016/j.mimet.2005.04.035

785 Plank M., 2022 Interaction of TOR and PKA Signaling in S. cerevisiae. Biomolecules 12: 210.
786 https://doi.org/10.3390/biom12020210

787 Quinlan A. R., and I. M. Hall, 2010 BEDTools: a flexible suite of utilities for comparing genomic
788 features. Bioinformatics 26: 841–842. https://doi.org/10.1093/bioinformatics/btq033

789 Rai M. N., C. Parsania, R. Rai, N. Shirgaonkar, K. Tan, *et al.*, 2021 Temporal transcriptional
790 response of Candida glabrata during macrophage infection reveals a multifaceted transcriptional
791 regulator CgXbp1 important for macrophage response and drug resistance. 2021.09.28.462173.

792 Reichmann D., W. Voth, and U. Jakob, 2018 Maintaining a Healthy Proteome during Oxidative
793 Stress. Mol. Cell 69: 203–213. https://doi.org/10.1016/j.molcel.2017.12.021

794 Rhind N., Z. Chen, M. Yassour, D. A. Thompson, B. J. Haas, *et al.*, 2011 Comparative
795 Functional Genomics of the Fission Yeasts. Science 332: 930–936.
796 https://doi.org/10.1126/science.1203357

797 Robinson M. D., D. J. McCarthy, and G. K. Smyth, 2010 edgeR: a Bioconductor package for
798 differential expression analysis of digital gene expression data. Bioinformatics 26: 139–140.
799 https://doi.org/10.1093/bioinformatics/btp616

800 Rodaki A., I. M. Bohovych, B. Enjalbert, T. Young, F. C. Odds, *et al.*, 2009 Glucose promotes
801 stress resistance in the fungal pathogen Candida albicans. Mol. Biol. Cell 20: 4845–4855.
802 https://doi.org/10.1091/mbc.e09-01-0002

803 Roetzer A., C. Gregori, A. M. Jennings, J. Quintin, D. Ferrandon, *et al.*, 2008 Candida glabrata
804 environmental stress response involves Saccharomyces cerevisiae Msn2/4 orthologous
805 transcription factors. Mol. Microbiol. 69: 603–620. https://doi.org/10.1111/j.1365-
806 2958.2008.06301.x

807 Romanowski K., A. Zaborin, V. Valuckaite, R. J. Rolfes, T. Babrowski, *et al.*, 2012 Candida
808 albicans Isolates from the Gut of Critically Ill Patients Respond to Phosphate Limitation by
809 Expressing Filaments and a Lethal Phenotype, (N. Chauhan, Ed.). PLoS ONE 7: e30119.
810 https://doi.org/10.1371/journal.pone.0030119

811 Saldanha A. J., M. J. Brauer, and D. Botstein, 2004 Nutritional homeostasis in batch and
812 steady-state culture of yeast. Mol. Biol. Cell 15: 4089–4104. https://doi.org/10.1091/mbc.E04-
813 04-0306

814 Scholz H., M. Franz, and U. Heberlein, 2005 The hangover gene defines a stress pathway
815 required for ethanol tolerance development. Nature 436: 845–847.
816 https://doi.org/10.1038/nature03864

817 Seider K., F. Gerwien, L. Kasper, S. Allert, S. Brunke, *et al.*, 2014 Immune Evasion, Stress
818 Resistance, and Efficient Nutrient Acquisition Are Crucial for Intracellular Survival of Candida
819 glabrata within Macrophages. Eukaryot. Cell 13: 170–183. https://doi.org/10.1128/EC.00262-13

820 Shen X.-X., D. A. Opulente, J. Kominek, X. Zhou, J. L. Steenwyk, *et al.*, 2018 Tempo and Mode
821 of Genome Evolution in the Budding Yeast Subphylum. Cell 175: 1533–1545.
822 https://doi.org/10.1016/j.cell.2018.10.023

823 Swinnen E., V. Wanke, J. Roosen, B. Smets, F. Dubouloz, *et al.*, 2006 Rim15 and the
824 crossroads of nutrient signalling pathways in Saccharomyces cerevisiae. Cell Div. 1: 3.
825 https://doi.org/10.1186/1747-1028-1-3

826 Urban J., A. Soulard, A. Huber, S. Lippman, D. Mukhopadhyay, *et al.*, 2007 Sch9 is a major
827 target of TORC1 in Saccharomyces cerevisiae. Mol. Cell 26: 663–674.
828 https://doi.org/10.1016/j.molcel.2007.04.020

829 Wanke V., I. Pedruzzi, E. Cameroni, F. Dubouloz, and C. De Virgilio, 2005 Regulation of G0
830 entry by the Pho80-Pho85 cyclin-CDK complex. EMBO J. 24: 4271–4278.
831 https://doi.org/10.1038/sj.emboj.7600889

832 Wanke V., E. Cameroni, A. Uotila, M. Piccolis, J. Urban, *et al.*, 2008 Caffeine extends yeast
833 lifespan by targeting TORC1. Mol. Microbiol. 69: 277–285. https://doi.org/10.1111/j.1365-
834 2958.2008.06292.x

835 Welker S., B. Rudolph, E. Frenzel, F. Hagn, G. Liebisch, *et al.*, 2010 Hsp12 is an intrinsically
836 unstructured stress protein that folds upon membrane association and modulates membrane
837 function. Mol. Cell 39: 507–520. https://doi.org/10.1016/j.molcel.2010.08.001

838 Wu Y., J. Wu, M. Deng, and Y. Lin, 2021 Yeast cell fate control by temporal redundancy
839 modulation of transcription factor paralogs. Nat. Commun. 12: 3145.
840 https://doi.org/10.1038/s41467-021-23425-0

841 Zakhem A. E., R. Istambouli, M. Alkozah, A. Gharamti, M. A. Tfaily, *et al.*, 2021 Predominance
842 of Candida Glabrata among Non-albicans Candida Species in a 16-Year Study of Candidemia
843 at a Tertiary Care Center in Lebanon. Pathog. Basel Switz. 10.
844 https://doi.org/10.3390/pathogens10010082

845 Zhou X., and E. K. O'Shea, 2011 Integrated approaches reveal determinants of genome-wide
846 binding and function of the transcription factor Pho4. Mol. Cell 42: 826–836.
847 https://doi.org/10.1016/j.molcel.2011.05.025

848

849 **Figure Legends**

850 **Figure 1. Phosphate starvation induces strong acquired resistance for H_2O_2 in *C. glabrata***
851 **and not in *S. cerevisiae*.** (A) Experimental design for quantifying Acquired Stress Resistance
852 (ASR): cells were first treated with phosphate starvation (-Pi, or P) or mock-treated (M), then
853 exposed to a secondary H_2O_2 (O) stress or a mock treatment (M). The resulting treatment
854 regimens were referred to as PO, MO, PM and MM. (B) and (C): cells after the four treatment
855 regimens were spotted on rich solid media and imaged after 24-48 hrs. Different H_2O_2
856 concentrations were used for the two species to achieve a similar survival rate without the primary
857 stress. (D) Survival rates (%) after the secondary H_2O_2 challenge were quantified using Colony
858 Forming Units either with (r') or without (r) phosphate starvation as a primary stress. The biological
859 replicates (n=8) were shown as dots and their means as bars. Basal survival rates (r) were not
860 different between species (P = 0.46), while there was a significant increase in survival due to the
861 primary stress in *C. glabrata* but not in *S. cerevisiae* (P-values = 0.0039 and 0.37, respectively).
862

863 **Figure 2. Phosphate starvation strongly induce many oxidative stress related genes in *C.***
864 ***glabrata* but not in *S. cerevisiae*.** (A) Proposed transcriptional basis for the acquired stress
865 resistance in *C. glabrata*: phosphate starvation induces both canonical phosphate homeostasis
866 genes and also oxidative stress response genes, providing protection for the secondary H_2O_2
867 challenge. (B) Known transcription factors (TFs) and effector gene categories involved in the
868 oxidative stress response (OSR) in *S. cerevisiae*. (C-F) Comparison of transcriptional induction
869 of genes known to be involved in OSR in *S. cerevisiae*. Log2 fold changes after 1 hour of
870 phosphate starvation were shown as the mean (bar) of 3 biological replicates (dots) for genes
871 encoding antioxidants (C), protease components (D), molecular chaperones (E) and TFs involved
872 in the OSR (F). The dotted lines indicate a 2 fold induction. Gene names were based on *S.*
873 *cerevisiae* except for *CTA1*, which had two paralogs in *S. cerevisiae* and only one in *C. glabrata*.
874 *S. cerevisiae CTT1* is involved in OSR and its fold change is shown in (C). Asterisks above a
875 gene name indicate that the gene was significantly induced in that species at an FDR of 0.05.
876

877 **Figure 3. *C. glabrata CTA1* is induced during phosphate starvation and is required for the**
878 **acquired resistance to severe H_2O_2 stress.** (A) *CTA1* mRNA levels were assayed using qRT-
879 PCR following 45 minutes of either 1.5 mM H_2O_2, phosphate starvation or mock treatment. Fold
880 changes over the mock treated samples were shown using *ACT1* as a reference. Two isogenic
881 lab strains of *C. glabrata* were each assayed in triplicates. Bars represent the mean of each strain.
882 An unpaired Student's t-test comparing the $\Delta\Delta C_T$ values between both treatments with the mock
883 found both to be significantly elevated (P < 0.01, strain was included as a covariate and found to
884 be not significant). (B) Cta1 protein levels were monitored in strains carrying a genomic *CTA*1-
885 GFP fusion using flow cytometry for 4 hours, during which cells were exposed to either mild H_2O_2
886 stress, phosphate starvation or mock treatment. The y-axis values are the median fluorescence
887 intensities (a.u. = arbitrary unit). The dots show the mean of >3 biological replicates; the error
888 bars show 95% confidence intervals based on bootstrapping and the lines are LOESS curves
889 fitted to the data. (C) ASR spotting assays for wild type and *cta1*Δ *C. glabrata* strains. 2.5 mM

890 H_2O_2 was used as the secondary stress for *cta1*Δ, which resulted in a similar basal survival rate
891 as 100 mM H_2O_2 for the wild type. (D) ASR effects were quantified by estimating the survival rates
892 after H_2O_2 treatments either with (solid circles) or without (open circles) the primary stress using
893 a colony forming unit (CFU) assay. The basal survival rates between the wild type and the *cta1*Δ
894 strain were not statistically different at the chosen concentrations (P = 0.39). Phosphate starvation
895 significantly increased the survival of both the wild type and the *cta1*Δ strain during the secondary
896 challenge (P = 0.016 in both cases), but the ASR effect size was dramatically lower in *cta1*Δ
897 (ASR-score = 9.8 and 1.5 in wild type and *cta1*Δ, respectively).
898
899 **Figure 4. TFs CgMsn4 and CgSkn7 jointly contribute to *CTA1* induction during phosphate**
900 **starvation in *C. glabrata*.** (A) Cta1-GFP levels over 4 hours of phosphate starvation for wild type
901 (WT) and TF deletion mutants. The dots represent the mean of > 3 biological replicates and the
902 error bars the 95% confidence interval based on 1000 bootstrap replicates. The lines are LOESS
903 fit to the data. (B) A schematic showing the predicted binding sites (BS) for Skn7 and Msn2/Msn4
904 in *C. glabrata* (Materials and Methods). Based on the prediction, two types of *cis*-mutants were
905 created: the internal deletions (4OL, 8OL) each removed 200 bp containing either the predicted
906 Msn2/Msn4 BS or both Skn7 BS; four point mutation alleles each targeted either the single
907 Msn2/Msn4 BS or one of the Skn7 BS predicted to have a higher affinity. (C, D) Comparing the
908 Cta1-GFP induction driven by each of the mutant promoters in (B) compared with the WT and the
909 corresponding TFΔ mutant.
910
911 **Figure 5. *C. glabrata* Msn4 (CgMsn4) translocates into the nucleus upon phosphate**
912 **starvation but not its ortholog in *S. cerevisiae* (ScMsn4).** Cellular localization of CgMsn4 (A)
913 and ScMsn4 (B) under phosphate starvation (-Pi), glucose starvation (-Glu), and no stress
914 conditions. All treatments were for 45 minutes. From left to right: i. CgMsn4-yeGFP and ScMsn4-
915 mCitrine; ii. nucleus staining with DAPI in *C. glabrata* or labeled with Nh6a-iRFP in *S. cerevisiae*;
916 iii. merge; iv. bright field. The percent of cells with nuclear-localized Msn4 and the total number of
917 cells examined by microscopy were shown on the right. Scale bars represent 5 μm in length.
918
919 **Figure 6. The Greatwall kinase homolog Rim15 mediates phosphate starvation-induced**
920 **ASR in *C. glabrata*.** (A) Proposed model for phosphate starvation-induced ASR in *C. glabrata*:
921 phosphate starvation (-Pi) activates Rim15, which goes on to regulate Msn4's activity and
922 contributes to ASR. Dashed arrows show proposed connections; solid arrows are regulations
923 supported by previous results; red question marks indicate specific downstream effects to be
924 tested. (B) CgMsn4 nuclear localization in WT and *rim15*Δ strains in -Pi or rich media. Left:
925 CgMsn4-GFP, % of cells with $CgMsn4^{nuc}$ labeled on the lower left; right: bright field (BF) showing
926 cells. Fisher's Exact Tests (FET) were performed to compare the two strains under each condition.
927 Raw, two-sided P-values were reported on the side. (C) Cta1-GFP induction during -Pi. Dots are
928 the means of >3 biological replicates and the error bars the 95% CI based on 1000 bootstraps.
929 (D) ASR assay for the wild type (WT) and *rim15*Δ. Shown are survival rates of the two strains at
930 an equivalent H_2O_2 strength (100 mM for WT and 80 mM for *rim15*Δ), either with (-Pi) or without
931 (Mock) a primary stress. Each dot is an independent biological replicate (n = 7) and the red bar

932 represents the mean. Basal survival rates were not different between the two strains (P = 0.5). A
933 Wilcoxon signed-rank test was used to assess the significance of the ASR. The raw, one-sided
934 P-values were 0.008 for both *WT* and *rim15*Δ. The ASR effect was significantly lower in *rim15*Δ
935 (mean ASR-score = 6.29 in WT and 3.45 in *rim15*Δ, respectively, Wilcoxon signed-rank test one-
936 sided P = 0.02).
937
938 **Figure 7. TORC1 is strongly inhibited by phosphate starvation in *C. glabrata*, likely**
939 **contributing to the ASR via its proximal kinase, Sch9.** (A) A representative Western Blot for
940 phosphorylated Rps6 (P-Rps6) and total Rps6 in both species under rich media, nitrogen
941 starvation (-N) or phosphate starvation (-Pi) conditions. Red arrows point to the loss vs presence
942 of the P-Rps6 band under -Pi in *C. glabrata* and *S. cerevisiae*, respectively. (B) Quantification
943 of %P-Rps6 over total Rps6 (n=3). *Bonferroni corrected P-values from Student's t-tests were
944 shown. (C) Inhibiting TORC1 by rapamycin induces Cta1-GFP in a dose-dependent manner. The
945 dots, error bars and lines have the same meaning as before. (D) Same plot comparing Cta1-GFP
946 induction in a phosphomimetic mutant of Sch9, a key proximal effector of TORC1, and a matching
947 wild type Sch9 strain. (E) ASR for H_2O_2 with rapamycin as the primary treatment. Plotted are
948 survival rates based on CFU. Red lines indicate means. Dotted lines connect paired experiments
949 with or without the primary treatment. A Wilcoxon signed-rank test was used to compare the two
950 groups and the raw P-values were shown on the top (lowest P-value possible with 4 replicates is
951 0.0625). (F) Same as E but with phosphate starvation (-Pi) as the primary stress, comparing the
952 Sch9-3E mutant and the matching Sch9-wt control. (G) Schematic summary of how TORC1
953 potentially mediates the -Pi induced ASR in *C. glabrata*. Dashed lines indicate regulatory links
954 based on *S. cerevisiae* studies; solid lines are regulations supported by genetic and
955 pharmacological perturbations in this study.
956
957 **Figure 8. ASR divergence and rewiring of the underlying regulatory network.** (A) Phosphate
958 starvation elicits a fast and strong induction of oxidative stress response (OSR) genes in *C.*
959 *glabrata* in addition to the canonical phosphate starvation response (right), providing strong
960 acquired resistance for a secondary H_2O_2 challenge; in the related *S. cerevisiae*, the induction of
961 OSR genes is much weaker and slower, explaining its lack of ASR. The orange arrows in the right
962 diagram indicate evolutionary rewiring in part of the response to phosphate limitation between the
963 two species. (B) Evolutionary rewiring at the transcriptional level. Regulation of OSR genes such
964 as *CTA1* involves some of the same transcription factors (TFs) during both oxidative stress and
965 phosphate starvation, but with different combinatorial logic. Width of the arrow indicates the
966 importance of the TF; the wide arrows to the right of the TFs indicate their combinatorial logic.
967 Asterisks indicate potential evolutionary events, both at the *trans*- and *cis*- (promoter)
968 levels. Combined, they lead to distinct induction kinetics under the two stimuli (right). (C)
969 Proposed rewiring in the Target-of-Rapamycin Complex 1 (TORC1). Nitrogen-sensing is
970 conserved between species and strongly activate two of TORC1's downstream branches. By
971 contrast, sensing of phosphate is evolutionarily labile; it strongly activates the stress response
972 branch but very weakly affects the nitrogen catabolism branch. The question mark indicates we
973 still lack direct evidence for TORC1 being responsible for the stress gene induction in the ASR.

974 This model suggests that flexibility in connecting individual stimulus with specific downstream
975 branch(es) allows TORC1 to contribute to the ASR evolution by avoiding pleiotropic effects.
976

977 **Tables**

978 **Table 1. Yeast strains used in this study**

Strain name	ID	Genotype	Source	Figure
C. glabrata BG99	yH181	[BG99]	[PMID: 10049916]	Fig. 1, 6
C. glabrata BG99 derivative	yH001; yH002	[BG99] ura3::pUC19; his3::pUC19		
S. cerevisiae K699	yH154	[W303] *MATa ade2-1 trp1-1 can 1-100 leu2-3,112 his3-11,15 ura3* GAL+		Fig. 1, 6
K. lactis	yH149	wild type		Fig. S6
L. waltii	yH217	wild type	Gift from Dr. Chris Hittinger	Fig. S6
CTA1-GFP	yH298; yH299	[BG99] *cta1::CTA1-GFP*	This study	Fig. 4
cta1Δ	yH271;y H272	[BG99] *cta1::URA3*	This study	Fig. S3, 4
cta1::CTA1	yH285; yH286	[BG99] *cta1::CgCTA1*	This study	Fig. S3
msn2Δ	yH417; yH418; yH419	[BG99] *msn2::HIS3; cta1::CTA1-GFP*	This study	Fig. 4
msn4Δ	yH429; yH430; yH431	[BG99] *msn4::NAT; cta1::CTA1-GFP*	This study	Fig. 4, 7
msn2Δ msn4Δ	yH433; yH434; yH435	[BG99] *msn2::HIS3; msn4::NAT; cta1::CTA1-GFP*	This study	Fig. 4
pho4Δ	yH005	[BG99] *pho4::URA3;*	This study	Fig. S3
rim15Δ	yH520; yH521; yH522	[BG99] *rim15::HIS3;*	This study	Fig. 6B

rim15Δ	yH609; yH610	[BG99] *rim15::HIS3; cta1::CTA1-GFP*	This study	Fig. 6C
msn4Δ rim15Δ	yH523; yH524; yH525	[BG99] *msn4::NAT; rim15::HIS3; cta1::CTA1-GFP*	This study	Fig. 7
skn7Δ	yH440; yH441; yH442	[BG99] *skn7::HIS3; cta1::CTA1-GFP*	This study	Fig. 4
yap1Δ	yH426	[BG99] *yap1::Nat*	This study	Fig. S3
yap1Δ	yH446; yH447; yH449	[BG99] *yap1::HIS3; cta1::CTA1-GFP*	This study	Fig. 4
msn4Δ skn7Δ	yH454; yH455; yH457	[BG99] *msn4::NAT; skn7::HIS3; cta1::CTA1-GFP*	This study	Fig. S4
yap1Δ skn7Δ	yH452; yH453	[BG99] *skn7::NAT; yap1::HIS3; cta1::CTA1-GFP*	This study	Fig. S4
4OL	yH352; yH355; yH356	[BG99] *200bp - 400bp upstream of translational start site of CTA1 removal ; cta1::CTA1-GFP*	This study	Fig. 4
8OL	yH340; yH341; yH342	[BG99] *600bp - 800bp upstream of translational start site of CTA1 removal ; cta1::CTA1-GFP*	This study	Fig. 4
muMsn4BS#1	yH353; yH354; yH355	[BG99] *Msn4 binding site mutation 1; cta1::CTA1-GFP*	This study	Fig. 4
muMsn4BS#2	yH384; yH385; yH386	[BG99] *Msn4 binding site mutation 2; cta1::CTA1-GFP*	This study	Fig. 4
muSkn7BS#1	yH403; yH404	[BG99] *Skn7 binding site mutation 1; cta1::CTA1-GFP*	This study	Fig. 4
muSkn7BS#2	yH405; yH406; yH407	[BG99] *Skn7 binding site mutation 1; cta1::CTA1-GFP*	This study	Fig. 4
ScMsn4-mCitrine ScMsn2-mcherry	yH223	[W303] Nhp6a-iRFP-Kan, Msn4-mCitrine(v163A)-spHIS5 Msn2-mCherry-Trp, *leu::PRS305*	[PMID: 27690227], gift from Dr.	Fig. 5

			Hao Nan	
ScDAL80pr-GFP	yH646; yH647; yH648	[BG99] *msn2::ScDal80pr-GFP*	This study	Fig. S9
C. glabrata budding assay	yH654	[BG99] pCU (pgrb2.1) CgPHo84p::yeGFP his3ter	This study	Fig. S11
S. cerevisiae budding assay	yH677	[S288C] Ura3::PHO84pr-GFP-URA3	This study	Fig. S11
Sch9-WT-Nat	yH692; yH693; yH694; yH695	[BG99] *sch9::Sch9-WT-Nat; cta1::CTA1-GFP*	This study	Fig. 7
Sch9-3E-Nat	yH699	[BG99] *sch9::Sch9-3E-Nat; cta1::CTA1-GFP*	This study	Fig. 7

979

980 **Table 2. Yeast expression plasmids used in this study**

Plasmids	**ID**	**Description**	**Source**	**Figure**
pCU-PDC1-GFP	pH078	CEN, URA3, yeGFP	PMID:23934995	
CgMsn4-GFP	pH153	pCU-PDC1-CgMsn4-yeGFP	This study	Fig. 5
CgMsn2-GFP	pH152	pCU-PDC1-CgMsn2-yeGFP	This study	Fig. S5
ScDAL80pr-GFP	pH306	pKW431-*ScDAL80pr*-yeGFP	This study	Fig. S9

981

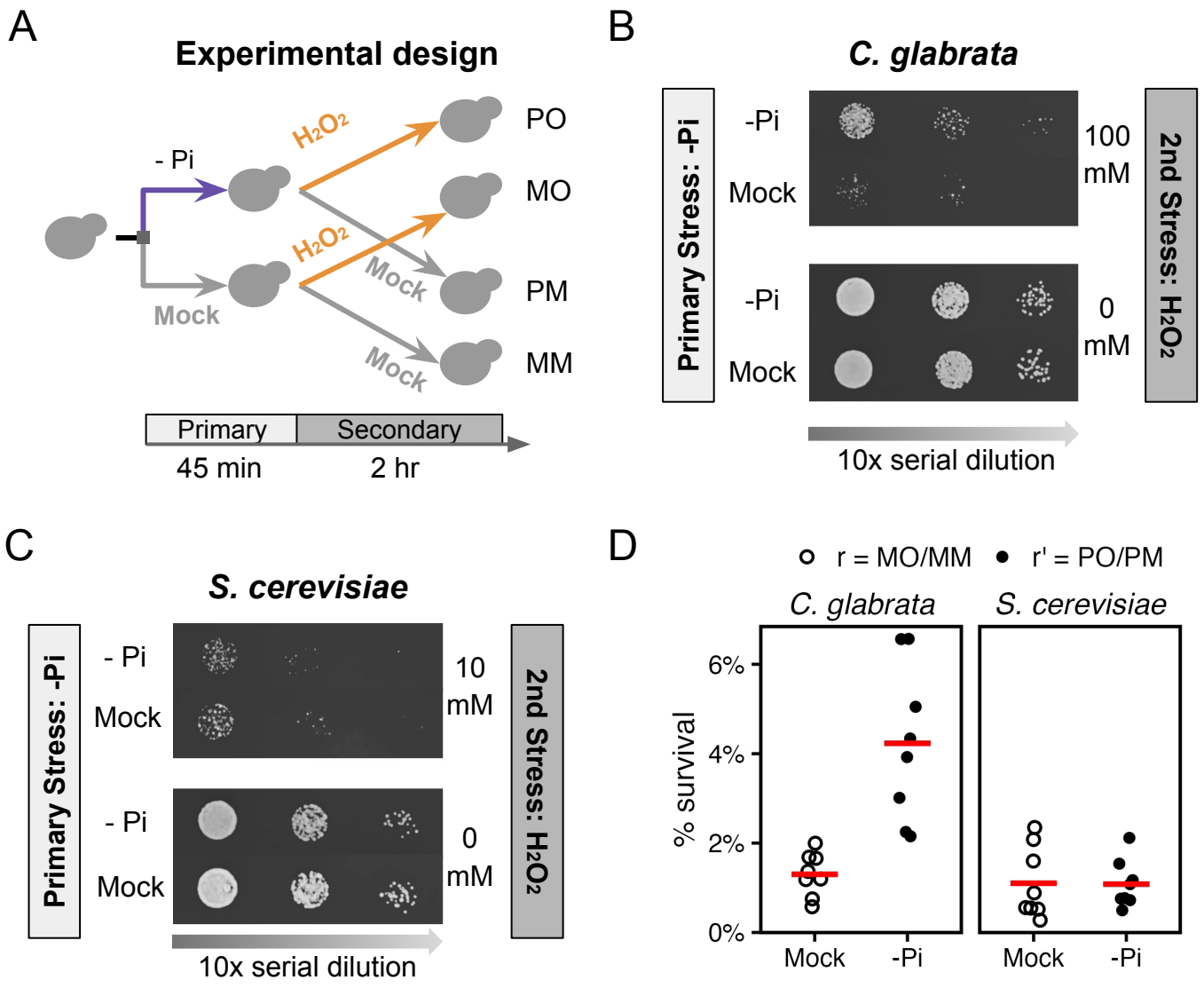

Figure 1. Phosphate starvation induces strong acquired resistance for H_2O_2 in *C. glabrata* and not in *S. cerevisiae*. (A) Experimental design for quantifying Acquired Stress Resistance (ASR): cells were first treated with phosphate starvation (-Pi, or P) or mock-treated (M), then exposed to a secondary H_2O_2 (O) stress or a mock treatment (M). The resulting treatment regimens were referred to as PO, MO, PM and MM. (B) and (C): cells after the four treatment regimens were spotted on rich solid media and imaged after 24-48 hrs. Different H_2O_2 concentrations were used for the two species to achieve a similar survival rate without the primary stress. (D) Survival rates (%) after the secondary H_2O_2 challenge were quantified using Colony Forming Units either with (r') or without (r) phosphate starvation as a primary stress. The biological replicates (n=8) were shown as dots and their means as bars. Basal survival rates (r) were not different between species (P = 0.46), while there was a significant increase in survival due to the primary stress in *C. glabrata* but not in *S. cerevisiae* (P-values = 0.0039 and 0.37, respectively).

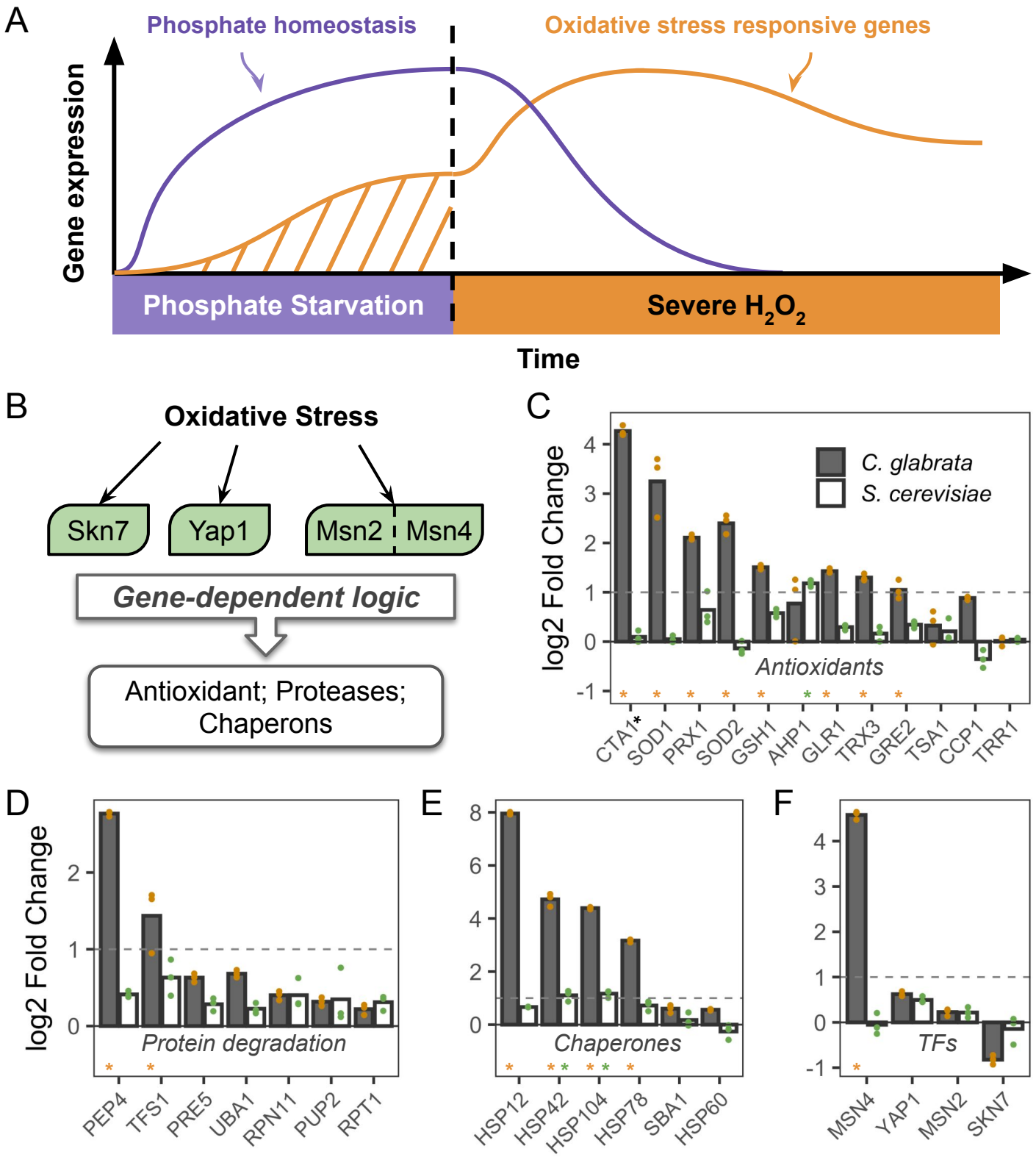

Figure 2. Phosphate starvation strongly induces many oxidative stress related genes in *C. glabrata* but not in *S. cerevisiae*. (A) Proposed transcriptional basis for the acquired stress resistance in *C. glabrata*: phosphate starvation induces both canonical phosphate homeostasis genes and also oxidative stress response genes, providing protection for the secondary H_2O_2 challenge. (B) Known transcription factors (TFs) and effector gene categories involved in the oxidative stress response (OSR) in *S. cerevisiae*. (C-F) Comparison of transcriptional induction of genes known to be involved in OSR in *S. cerevisiae*. Log2 fold changes after 1 hour of phosphate starvation were shown as the mean (bar) of 3 biological replicates (dots) for genes encoding antioxidants (C), protease components (D), molecular chaperones (E) and TFs involved in the OSR (F). The dotted lines indicate a 2 fold induction. Gene names were based on *S. cerevisiae* except for *CTA1*, which had two paralogs in *S. cerevisiae* and only one in *C. glabrata*. *S. cerevisiae CTT1* is involved in OSR and its fold change is shown in (C). Asterisks above a gene name indicate that the gene was significantly induced in that species at an FDR of 0.05.

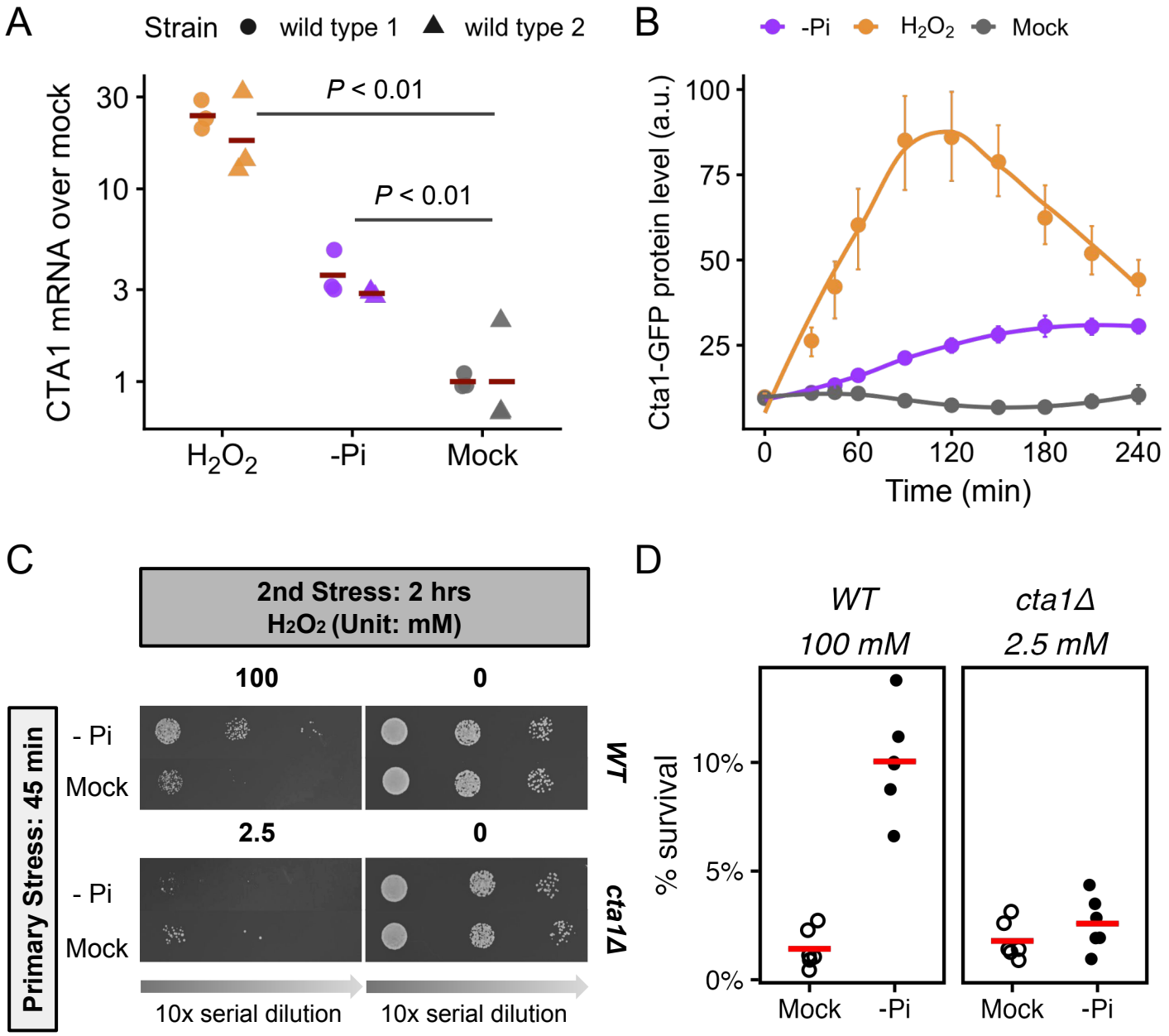

Figure 3. *C. glabrata CTA1* is induced during phosphate starvation and is required for the acquired resistance to severe H_2O_2 stress. (A) *CTA1* mRNA levels were assayed using qRT-PCR following 45 minutes of either 1.5 mM H_2O_2, phosphate starvation or mock treatment. Fold changes over the mock treated samples were shown using *ACT1* as a reference. Two isogenic lab strains of *C. glabrata* were each assayed in triplicates. Bars represent the mean of each strain. An unpaired Student's t-test comparing the $\Delta\Delta C_T$ values between both treatments with the mock found both to be significantly elevated ($P < 0.01$, strain was included as a covariate and found to be not significant). (B) Cta1 protein levels were monitored in strains carrying a genomic *CTA*1-GFP fusion using flow cytometry for 4 hours, during which cells were exposed to either mild H_2O_2 stress, phosphate starvation or mock treatment. The y-axis values are the median fluorescence intensities (a.u. = arbitrary unit). The dots show the mean of >3 biological replicates; the error bars show 95% confidence intervals based on bootstrapping and the lines are LOESS curves fitted to the data. (C) ASR spotting assays for wild type and *cta1*Δ *C. glabrata* strains. 2.5 mM H_2O_2 was used as the secondary stress for *cta1*Δ, which resulted in a similar basal survival rate as 100 mM H_2O_2 for the wild type. (D) ASR effects were quantified by estimating the survival rates after H_2O_2 treatments either with (solid circles) or without (open circles) the primary stress using a colony forming unit (CFU) assay. The basal survival rates between the wild type and the *cta1*Δ strain were not statistically different at the chosen concentrations ($P = 0.39$). Phosphate starvation significantly increased the survival of both the wild type and the *cta1*Δ strain during the secondary challenge ($P = 0.016$ in both cases), but the ASR effect size was much smaller in *cta1*Δ (ASR-score = 9.8 and 1.5 in wild type and *cta1*Δ, respectively).

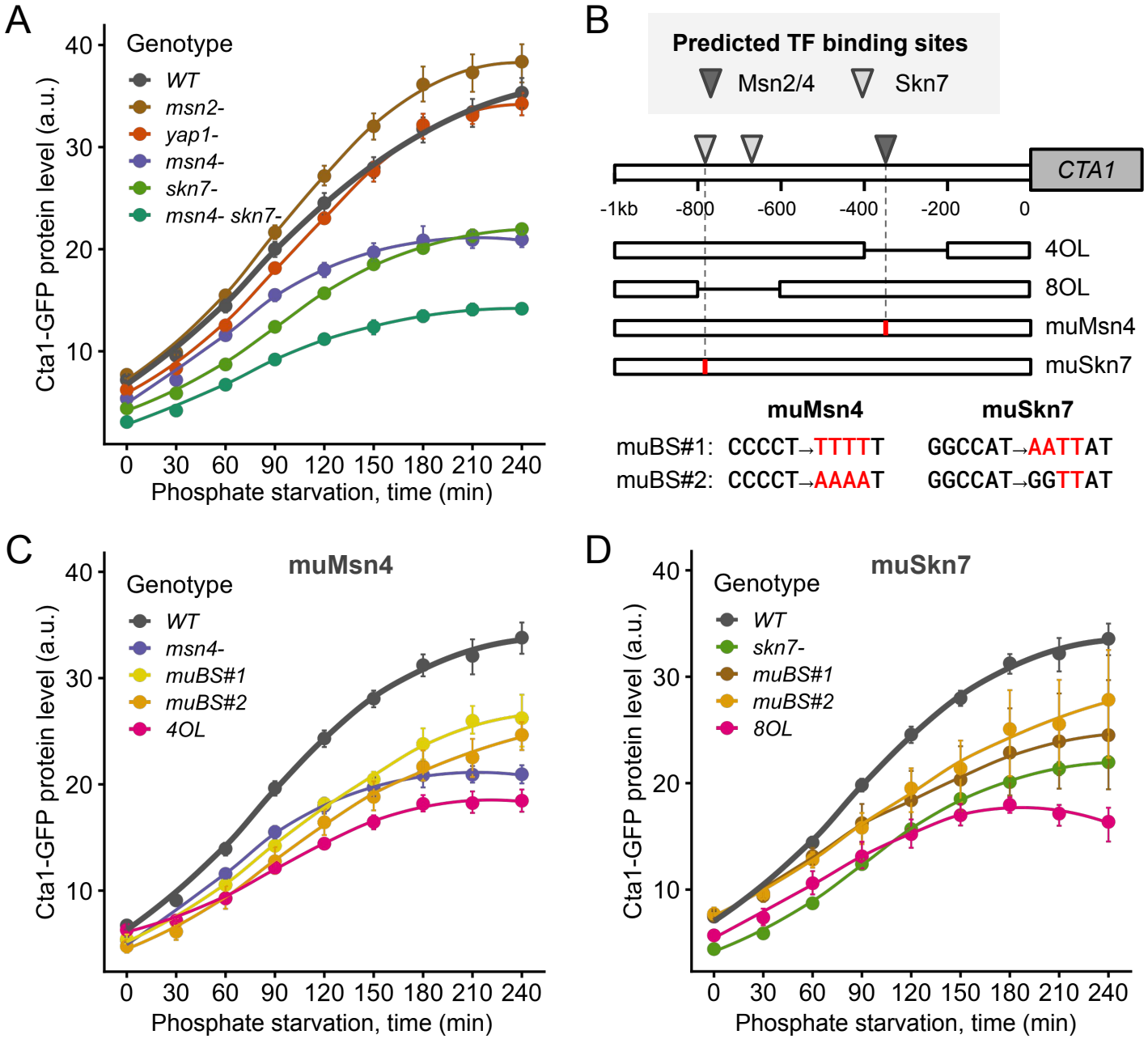

Figure 4. TFs CgMsn4 and CgSkn7 jointly contribute to *CTA1* induction during phosphate starvation in *C. glabrata*. (A) Cta1-GFP levels over 4 hours of phosphate starvation for wild type (WT) and TF deletion mutants. The dots represent the mean of > 3 biological replicates and the error bars the 95% confidence interval based on 1000 bootstrap replicates. The lines are LOESS fit to the data. (B) A schematic showing the predicted binding sites (BS) for Skn7 and Msn2/Msn4 in *C. glabrata* (Materials and Methods). Based on the prediction, two types of *cis*-mutants were created: the internal deletions (4OL, 8OL) each removed 200 bp containing either the predicted Msn2/Msn4 BS or both Skn7 BS; four point mutation alleles each targeted either the single Msn2/Msn4 BS or one of the Skn7 BS predicted to have a higher affinity. (C, D) Comparing the Cta1-GFP induction driven by each of the mutant promoters in (B) compared with the WT and the corresponding TFΔ mutant.

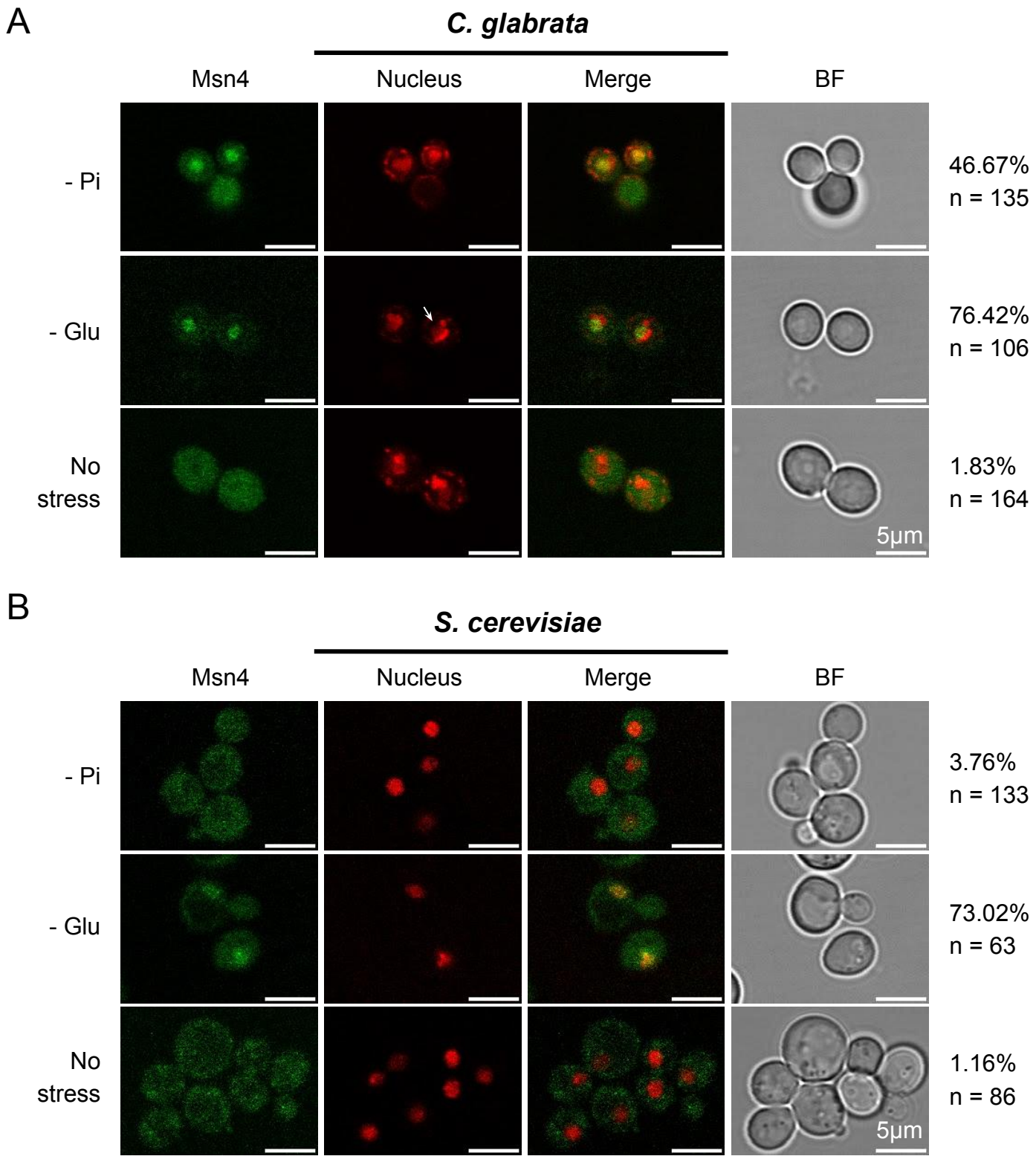

Figure 5. *C. glabrata* Msn4 (CgMsn4) translocates into the nucleus upon phosphate starvation but not its ortholog in *S. cerevisiae* (ScMsn4). Cellular localization of CgMsn4 (A) and ScMsn4 (B) under phosphate starvation (-Pi), glucose starvation (-Glu), and no stress conditions. All treatments were for 45 minutes. From left to right: i. CgMsn4-yeGFP and ScMsn4-mCitrine; ii. nucleus staining with DAPI in *C. glabrata* or labeled with Nh6a-iRFP in *S. cerevisiae*; iii. merge; iv. bright field. The percent of cells with nuclear-localized Msn4 and the total number of cells examined by microscopy were shown on the right. Scale bars represent 5 μm in length.

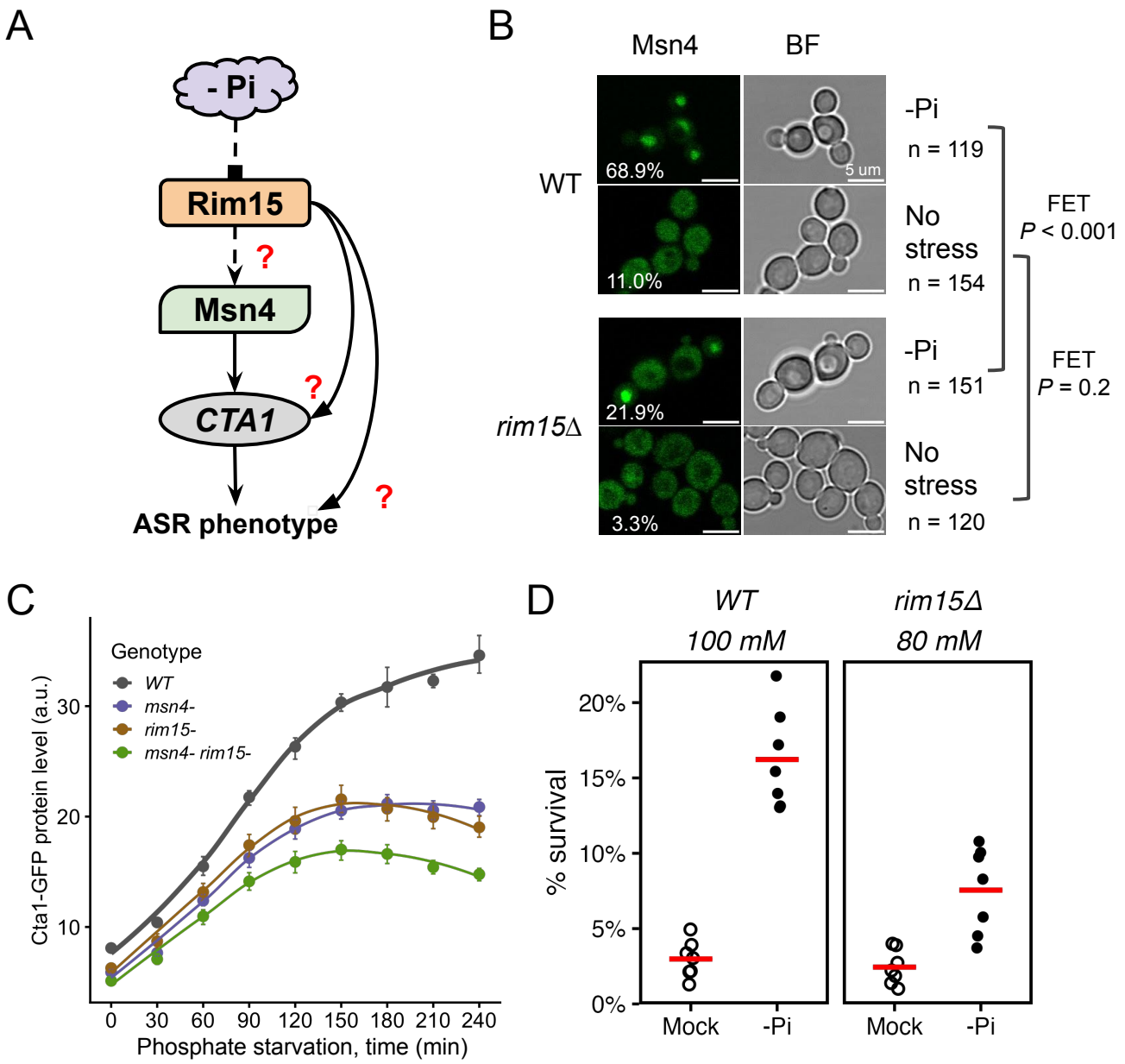

Figure 6. The Greatwall kinase homolog Rim15 mediates phosphate starvation-induced ASR in *C. glabrata*. (A) Proposed model for phosphate starvation-induced ASR in *C. glabrata*: phosphate starvation (-Pi) activates Rim15, which goes on to regulate Msn4's activity and contributes to ASR. Dashed arrows show proposed connections; solid arrows are regulations supported by previous results; red question marks indicate specific downstream effects to be tested. (B) CgMsn4 nuclear localization in WT and *rim15*Δ strains in -Pi or rich media. Left: CgMsn4-GFP, % of cells with CgMsn4^{nuc} labeled on the lower left; right: bright field (BF) showing cells. Fisher's Exact Tests (FET) were performed to compare the two strains under each condition. Raw, two-sided *P*-values were reported on the side. (C) Cta1-GFP induction during -Pi. Dots are the means of >3 biological replicates and the error bars the 95% CI based on 1000 bootstraps. (D) ASR assay for the wild type (WT) and *rim15*Δ. Shown are survival rates of the two strains at an equivalent H_2O_2 strength (100 mM for WT and 80 mM for *rim15*Δ), either with (-Pi) or without (Mock) a primary stress. Each dot is an independent biological replicate (n = 7) and the red bar represents the mean. Basal survival rates were not different between the two strains (*P* = 0.5). A Wilcoxon signed-rank test was used to assess the significance of the ASR. The raw, one-sided *P*-values were 0.008 for both *WT* and *rim15*Δ. The ASR effect was significantly lower in *rim15*Δ (mean ASR-score = 6.29 in WT and 3.45 in *rim15*Δ, respectively, Wilcoxon signed-rank test one-sided *P* = 0.02).

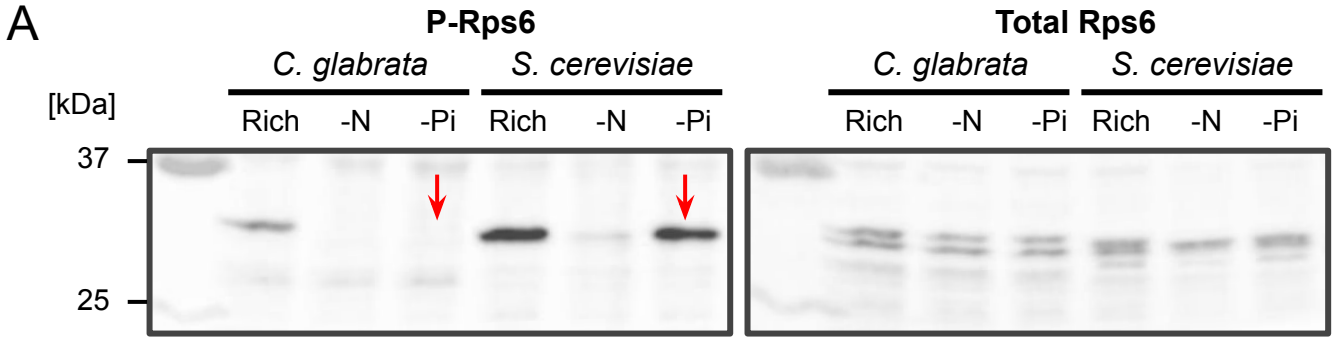

B

	C. glabrata			*S. cerevisiae*		
	Rich	-N	-Pi	Rich	-N	-Pi
P-Rps6 / total Rps6 (mean ± sd, n = 3)	2.9 ± 0.7	0.05 ± 0.05	0.04 ± 0.08	1.8 ± 0.5	0.4 ± 0.3	2.9 ± 1.6
***P*-value* vs Rich**	N/A	0.06	0.06	N/A	0.07	1

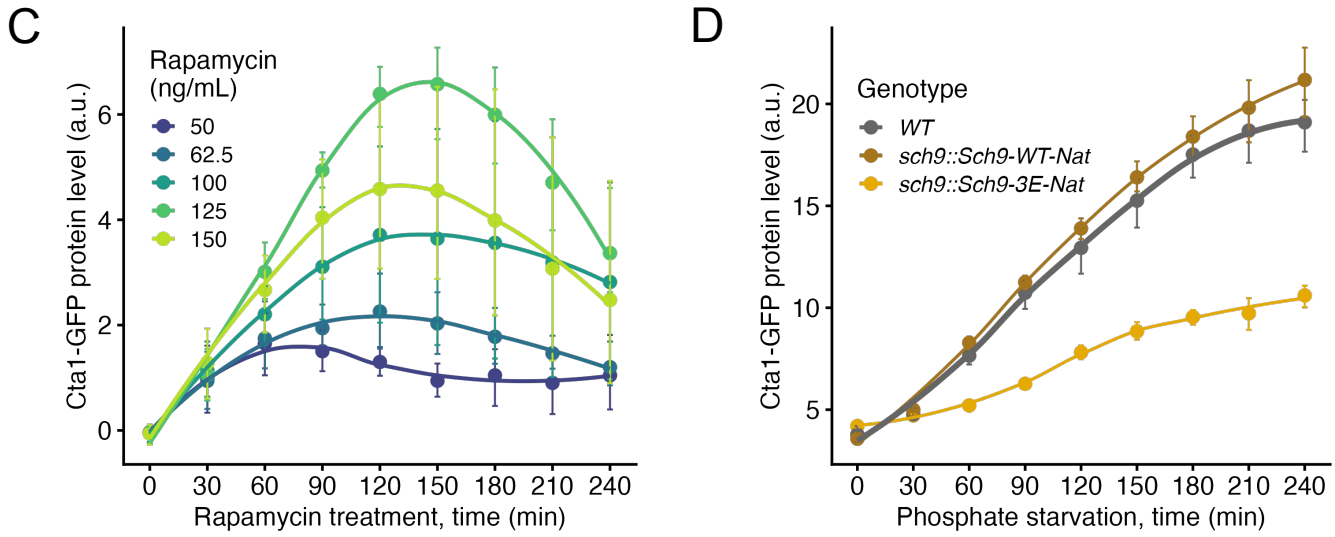

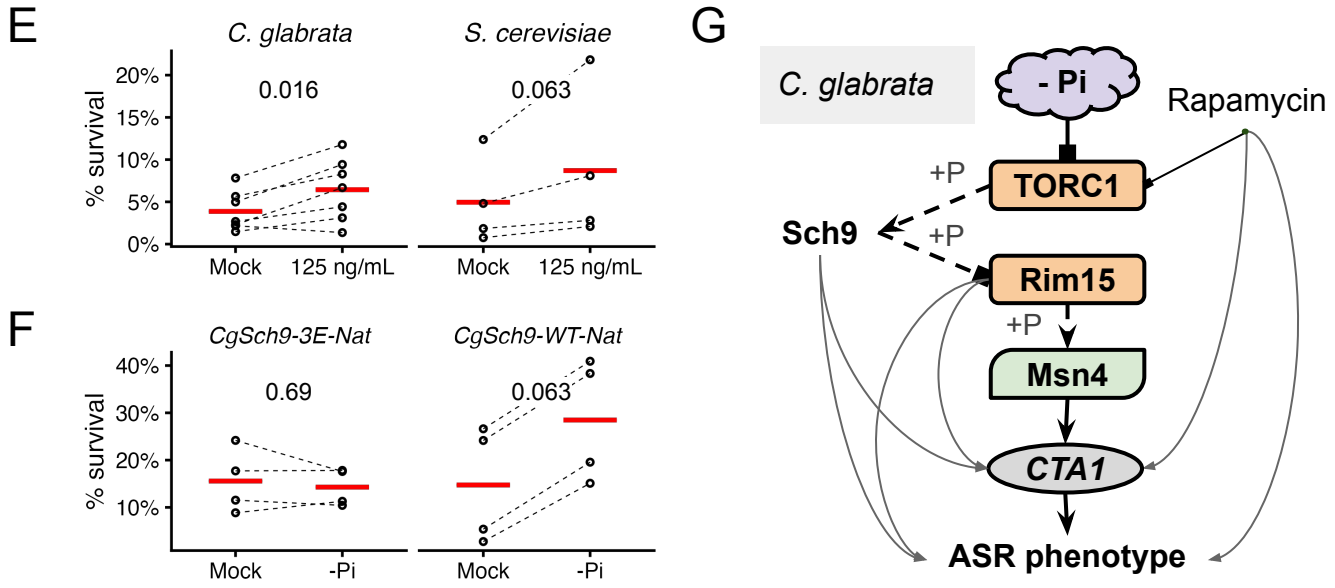

Figure 7. TORC1 is strongly inhibited by phosphate starvation in *C. glabrata*, likely contributing to the ASR via its proximal kinase, Sch9. see after Figure 8 for legends.

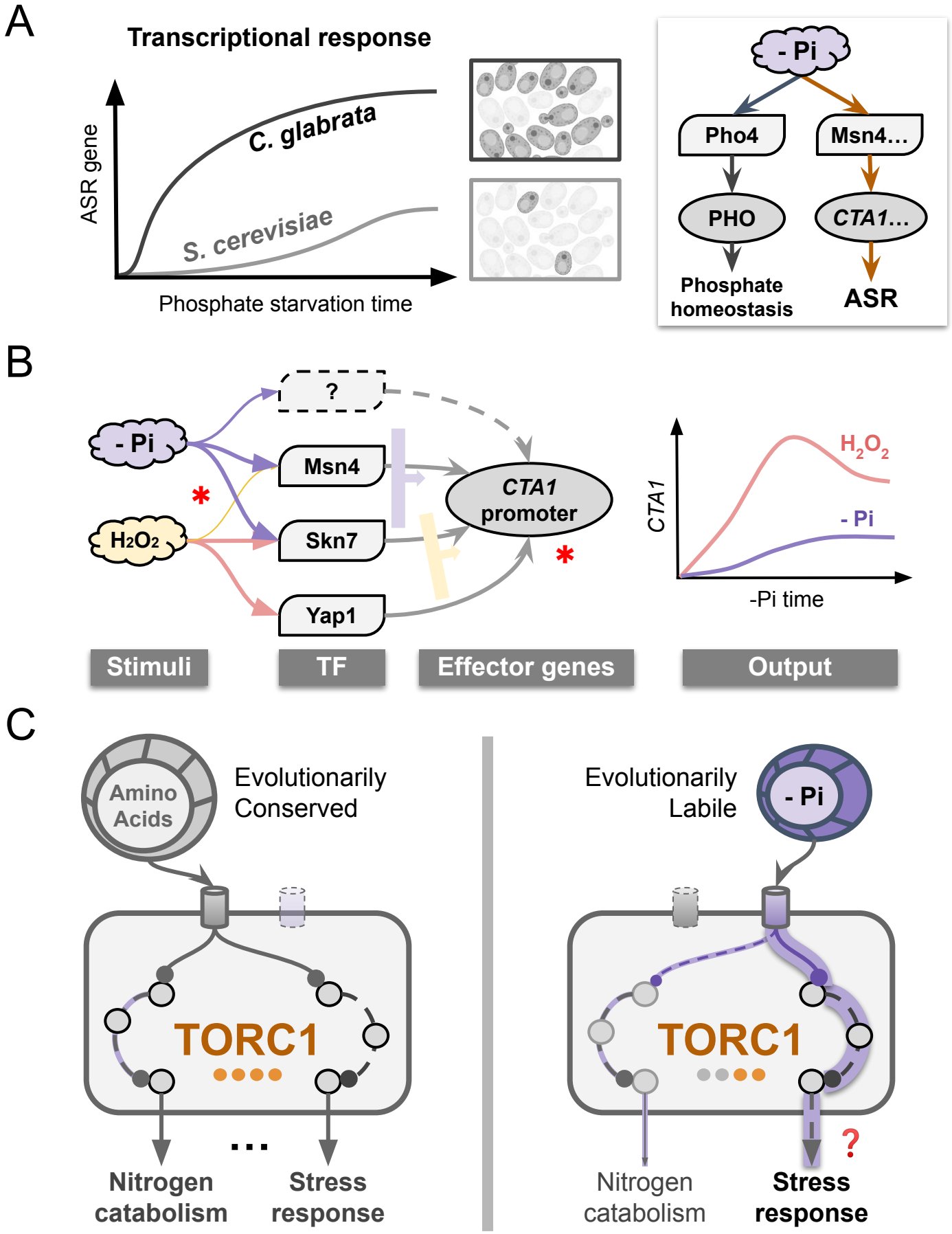

Figure 8. ASR divergence and rewiring of the underlying regulatory network. See next page for legend

Figure 7. TORC1 is strongly inhibited by phosphate starvation in *C. glabrata*, likely contributing to the ASR via its proximal kinase, Sch9. (A) A representative Western Blot for phosphorylated Rps6 (P-Rps6) and total Rps6 in both species under rich media, nitrogen starvation (-N) or phosphate starvation (-Pi) conditions. Red arrows point to the loss vs presence of the P-Rps6 band under -Pi in *C. glabrata* and *S. cerevisiae*, respectively. (B) Quantification of %P-Rps6 over total Rps6 (n=3). *Bonferroni corrected *P*-values from Student's t-tests were shown. (C) Inhibiting TORC1 by rapamycin induces Cta1-GFP in a dose-dependent manner. The dots, error bars and lines have the same meaning as before. (D) Same plot comparing Cta1-GFP induction in a phosphomimetic mutant of Sch9, a key proximal effector of TORC1, and a matching wild type Sch9 strain. (E) ASR for H_2O_2 with rapamycin as the primary treatment. Plotted are survival rates based on CFU (n=12 for *C. glabrata*, n=8 for *S. cerevisiae*). Red lines indicate means. Dotted lines connect paired experiments with or without the primary treatment. A Wilcoxon signed-rank test was used to compare the two groups and the raw *P*-values were shown on the top. (F) Same as E but with phosphate starvation (-Pi) as the primary stress, comparing the Sch9-3E mutant (n=4) and the matching Sch9-wt control (n=4). (G) Schematic summary of how TORC1 potentially mediates the -Pi induced ASR in *C. glabrata*. Dashed lines indicate regulatory links based on *S. cerevisiae* studies; solid lines are regulations supported by genetic and pharmacological perturbations in this study.

Figure 8. ASR divergence and rewiring of the underlying regulatory network. (A) Phosphate starvation elicits a fast and strong induction of oxidative stress response (OSR) genes in *C. glabrata* in addition to the canonical phosphate starvation response (right), providing strong acquired resistance for a secondary H_2O_2 challenge; in the related *S. cerevisiae*, the induction of OSR genes is much weaker and slower, explaining its lack of ASR. The orange arrows in the right diagram indicate evolutionary rewiring in part of the response to phosphate limitation between the two species. (B) Evolutionary rewiring at the transcriptional level. Regulation of OSR genes such as *CTA1* involves some of the same transcription factors (TFs) during both oxidative stress and phosphate starvation, but with different combinatorial logic. Width of the arrow indicates the importance of the TF; the wide arrows to the right of the TFs indicate their combinatorial logic. Asterisks indicate potential evolutionary events, both at the *trans*- and *cis*- (promoter) levels. Combined, they lead to distinct induction kinetics under the two stimuli (right). (C) Proposed rewiring in the Target-of-Rapamycin Complex 1 (TORC1). Nitrogen-sensing is conserved between species and strongly activate two of TORC1's downstream branches. By contrast, sensing of phosphate is evolutionarily labile; it strongly activates the stress response branch but very weakly affects the nitrogen catabolism branch. The question mark indicates we still lack direct evidence for TORC1 being responsible for the stress gene induction in the ASR. This model suggests that flexibility in connecting individual stimulus with specific downstream branch(es) allows TORC1 to contribute to the ASR evolution by avoiding potential pleiotropic effects.

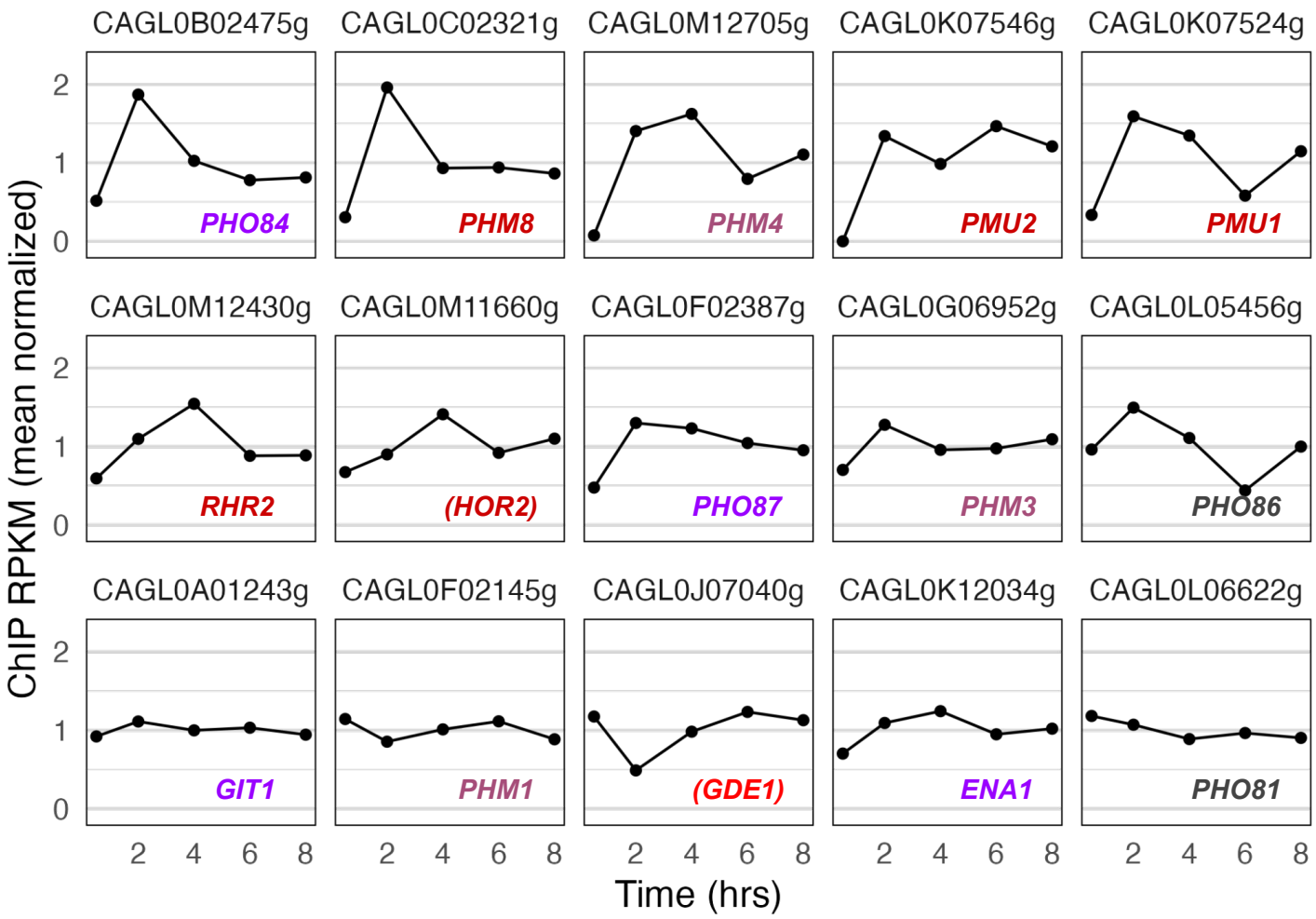

Phosphate transporters; Phosphatases; Phosphodiesterase; polyphosphate metabolism; regulatory

Supplementary Figure 1. Phosphate starvation response is partially induced in *C. glabrata* after the yeast is engulfed by human macrophages. Shown are the phosphate homeostasis genes induced during phosphate starvation in *C. glabrata*. Gene list is from (He *et al.* 2017). PolII ChIP-seq time course data are from (Rai *et al.* 2021), sampled at 0.5h, 2h, 4h, 6h and 8h post infection. For each gene, the ChIP-seq RPKM values were divided by the mean such that the normalized values represent fold changes over the mean for that gene. Systematic gene IDs were labeled on the top of each panel. Gene names were shown inside the panel (names in parentheses were based on *S. cerevisiae* homologs). Colors represented gene functional categories as explained below.

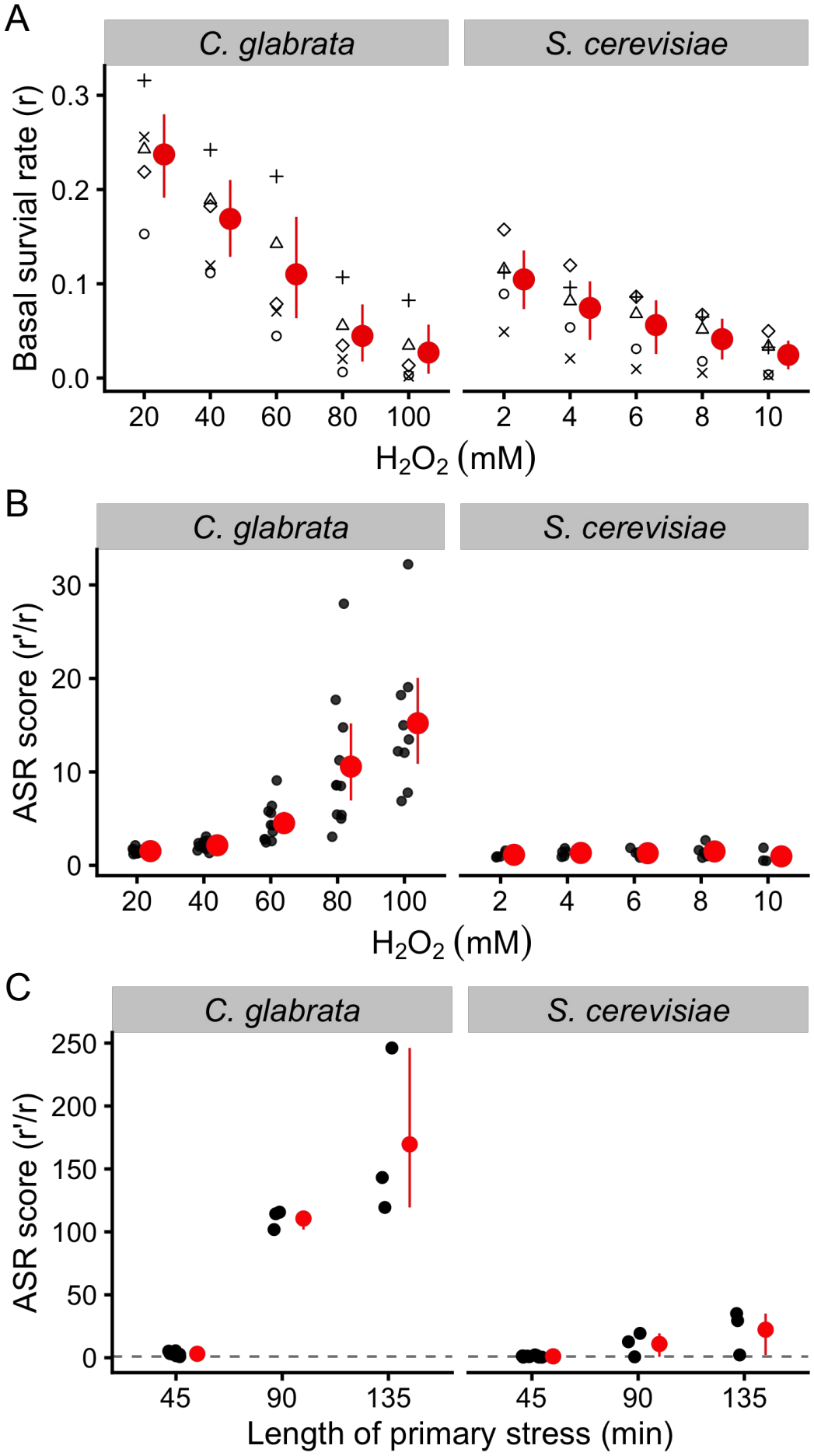
A
C. glabrata
S. cerevisiae
Basal survial rate (r)
0.3
0.2
0.1
0.0
20
40
60
80
100
2
4
6
8
10
H2O2 (mM)
B
C. glabrata
S. cerevisiae
ASR score (r'/r)
30
20
10
0
20
40
60
80
100
2
4
6
8
10
H2O2 (mM)
C
C. glabrata
S. cerevisiae
ASR score (r'/r)
250
200
150
100
50
0
45
90
135
45
90
135
Length of primary stress (min)

Supplementary Figure 2. Basal survival rates and phosphate starvation induced acquired resistance for H_2O_2 at different primary and secondary stress conditions. (A) Basal survival rates (r) at different H_2O_2 concentrations in *C. glabrata* and *S. cerevisiae* were quantified using Colony Forming Unit (CFU) ratios between cells treated with H_2O_2 and mock treated ones. The red dots and vertical lines show the mean and 95% confidence intervals based on 1000 bootstrap replicates. Individual data points are shown in different shapes grouped by the date of the experiment. (B) Acquired Stress Resistance (ASR) at different H_2O_2 secondary stress levels in the two species. ASR-score is defined as the fold increase in survival after the H_2O_2 treatment as a result of the primary stress (phosphate starvation). r' is the survival rate with the primary stress and r is the same as in (A), i.e., without the primary stress. The red dots and lines have the same meanings as in (A). (C) ASR for H_2O_2 at different primary stress length. 100 mM and 10 mM of H_2O_2 were used as the secondary stress for the two species as in Fig. 1. The dotted line shows an ASR score of 1 (i.e., no increase in survival due to the primary stress). A paired t-test was performed on the underlying survival rates (r and r') for each of the six species-by-duration combinations. After Bonferroni correction, all three tests in *C. glabrata* had $P < 0.05$, while all three tests in *S. cerevisiae* yielded $P > 0.5$

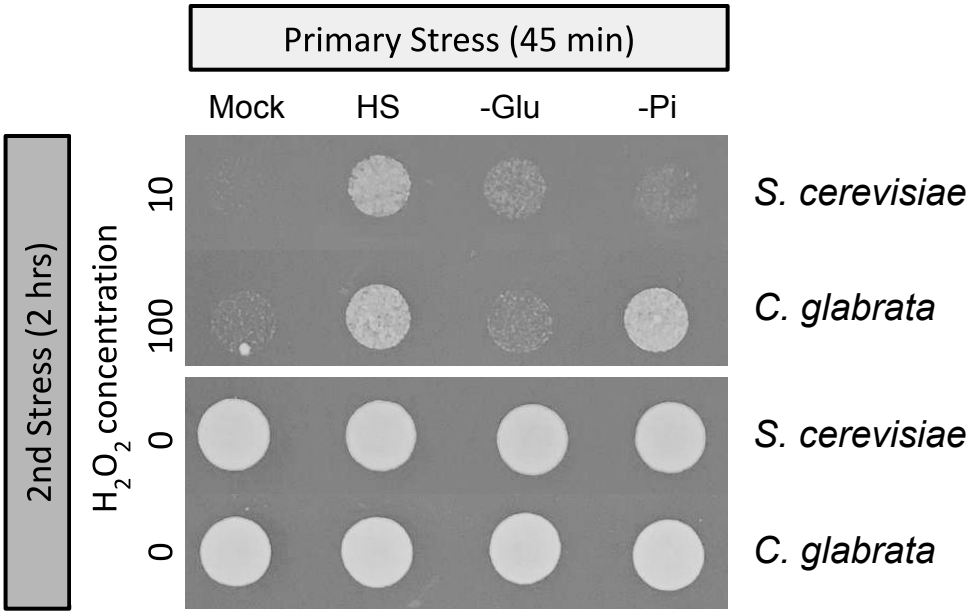

Supplementary Figure 3. Phosphate starvation-induced ASR for H_2O_2 diverge between species while other primary stresses show similar effects. ASR experiment was performed as in Figure 1, with the exception of using different primary stresses as indicated on the top: Mock - rich SC medium; HS - Heat shock at 43C; -Glu - 0.05% glucose (as opposed to 2% in SC); -Pi - no phosphate SC medium. Images were taken 14 hrs and 21 hrs post spotting for *C. glabrata* and *S. cerevisiae* respectively.

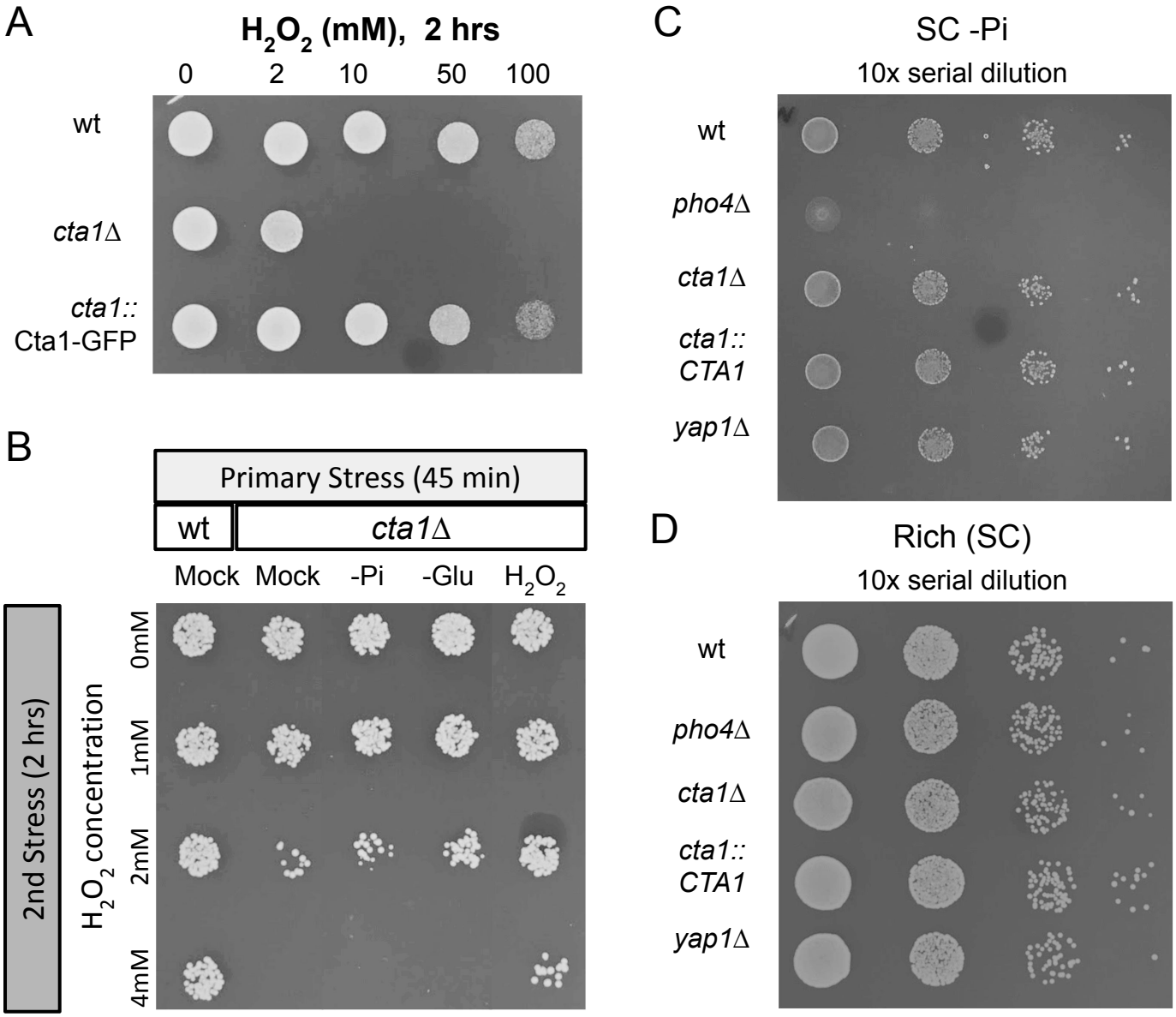

Supplementary Figure 4. Spotting assay for Cta1-GFP and *cta1*Δ strains in H_2O_2, ASR and phosphate starvation. (A) Endogenously-tagged Cta1-GFP showed no defect under H_2O_2 stress. *C. glabrata* wild type, *cta1*Δ and *cta1::*Cta1-GFP strains were treated at the indicated concentrations of H_2O_2 for 2 hours, then spotted onto YPD plates and incubated at 30°C for 48 hours. (B) *CTA1*'s importance for ASR is dependent on the primary stress type. ASR for wild type and *cta1*Δ were tested with various primary stresses, including phosphate starvation (-Pi), glucose starvation (-Glu, 0.02% as opposed to 2% glucose in SC), mild H_2O_2 (1.5 mM H_2O_2). ASR experiment was performed as described in the text. (C) Deleting *cta1* and the OSR TF, *yap1*, had no defect on survival under phosphate starvation, while deletion of *pho4*, which is responsible for the PHO response, showed severe growth defects. Mid-log phase cells of the indicated genotypes were spotted on no phosphate SC plates, incubated at 30°C for 48 hours. (D) Same as (C) but spotted onto SC plates with 7.5 mM Pi. All images are representatives of >3 biological replicates.

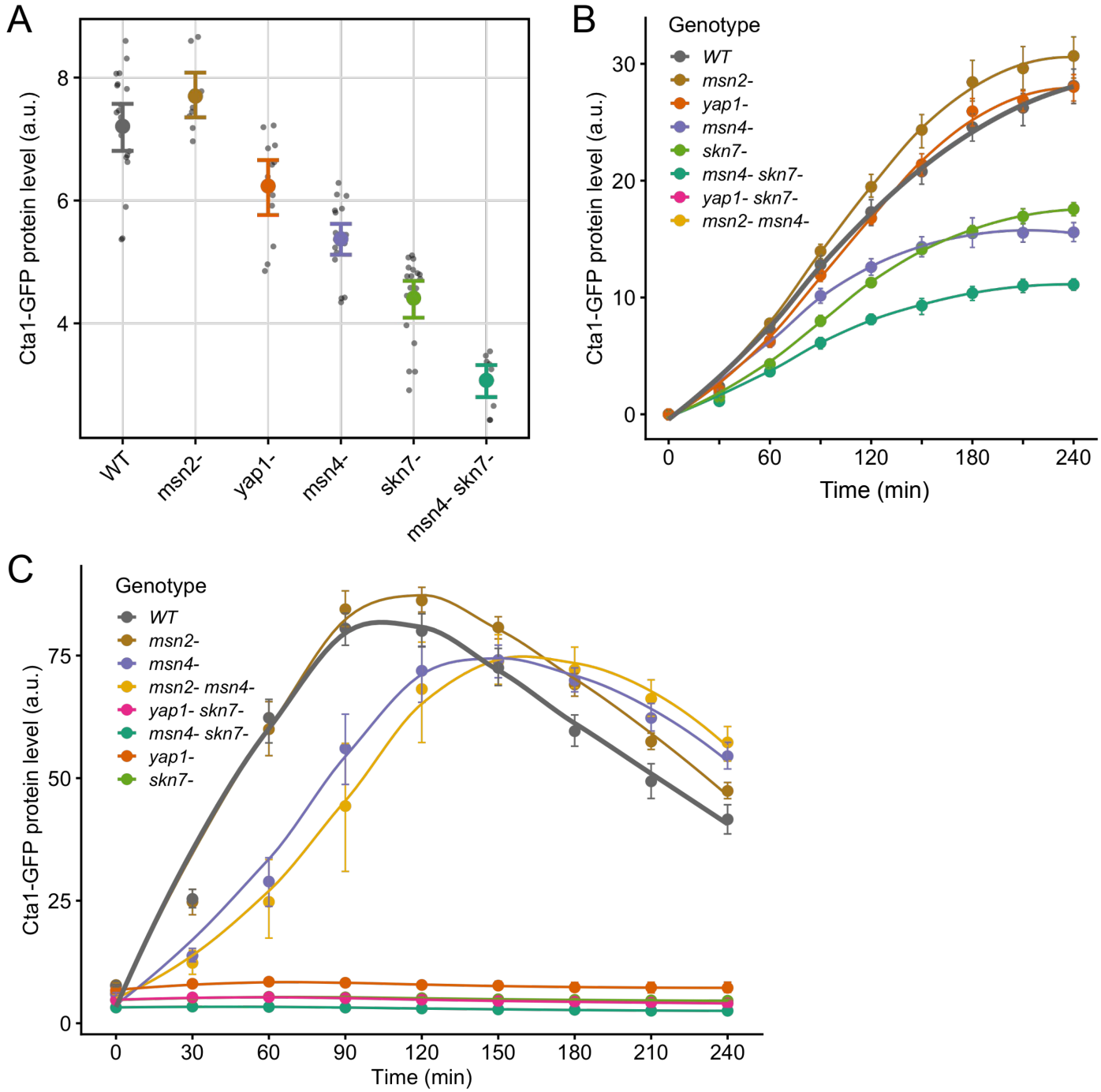

Supplementary Figure 5. TFΔ effects on Cta1-GFP induction under phosphate starvation and H_2O_2 stress. (A) Cta1-GFP levels prior to the onset of phosphate starvation. Each gray dot is an independent experiment. The large dot in the center and the error bars represent the mean and 95% confidence interval based on 1000 bootstrap replicates. All mutants except for *msn2*Δ had significantly lower basal Cta1-GFP levels at a 0.05 level after Bonferroni correction. (B) The same plot as in Figure 4A except that the 0 min mean levels were subtracted from all time points for each genotype to remove the differences in basal level expression. (C) Cta1-GFP induction under 2 mM H_2O_2 for 4 hours. Same features as in (B) and Figure 4A.

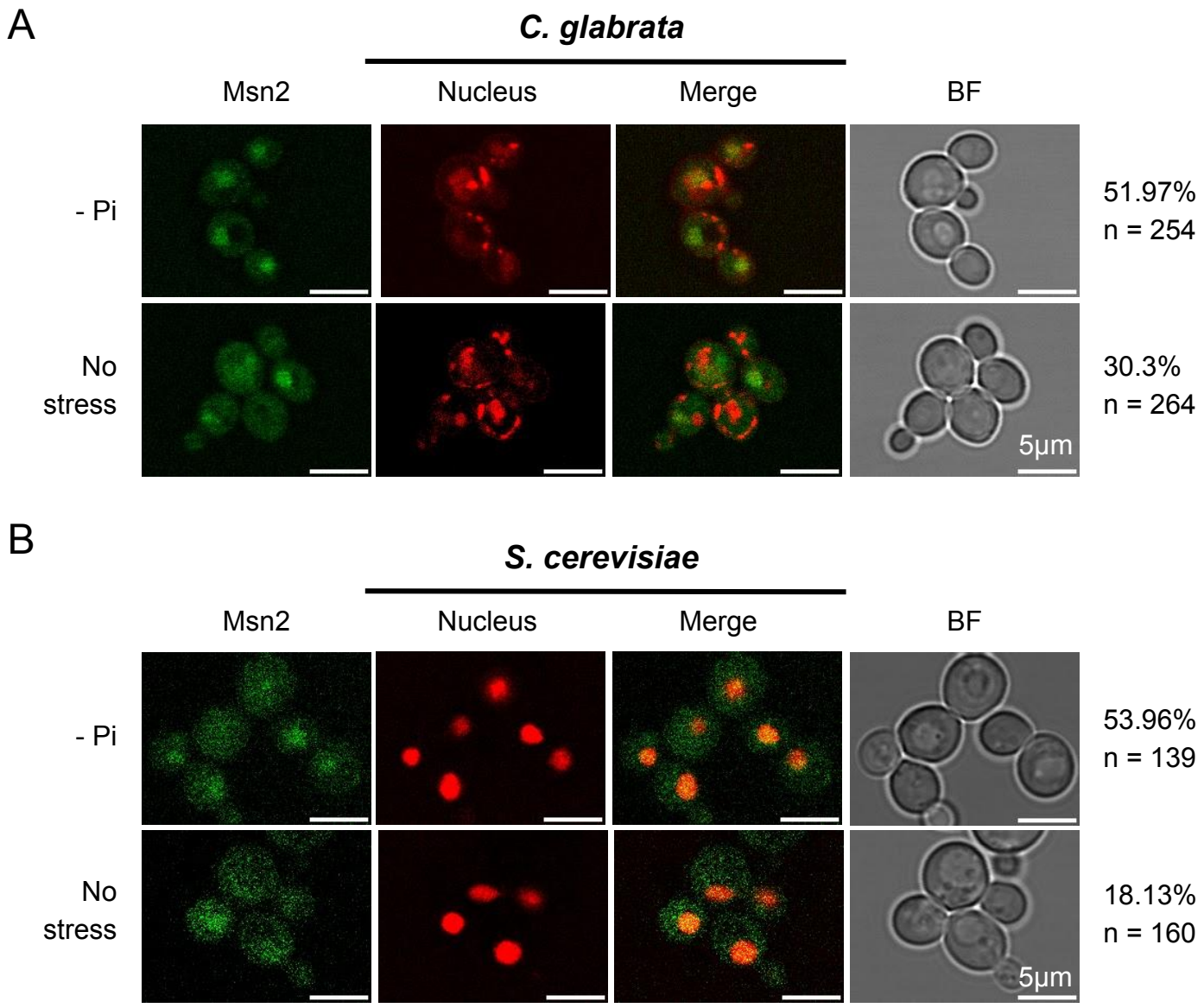

Supplementary Figure 6. *C. glabrata* Msn2 (CgMsn2) and *S. cerevisiae* Msn2 (ScMsn2) translocates into the nucleus upon phosphate starvation. Cellular localization of CgMsn2 (A) and ScMsn2 (B) under phosphate starvation (-Pi) and no stress conditions. All treatments were for 45 minutes. From left to right: i. CgMsn2-yeGFP and ScMsn2-mCherry (pseudo color); ii. nucleus staining with DAPI in *C. glabrata* or Nh6a-iRFP in *S. cerevisiae*; iii. merge of i and ii; iv. bright field; v. percentage of cells with nuclear-localized CgMsn2 or ScMsn2 under each condition (n=number of cells quantified). Scale bars all represent 5 µm in length. DAPI stained more than the nucleus in living *C. glabrata* cells as observed by others (Roetzer *et al.* 2008).

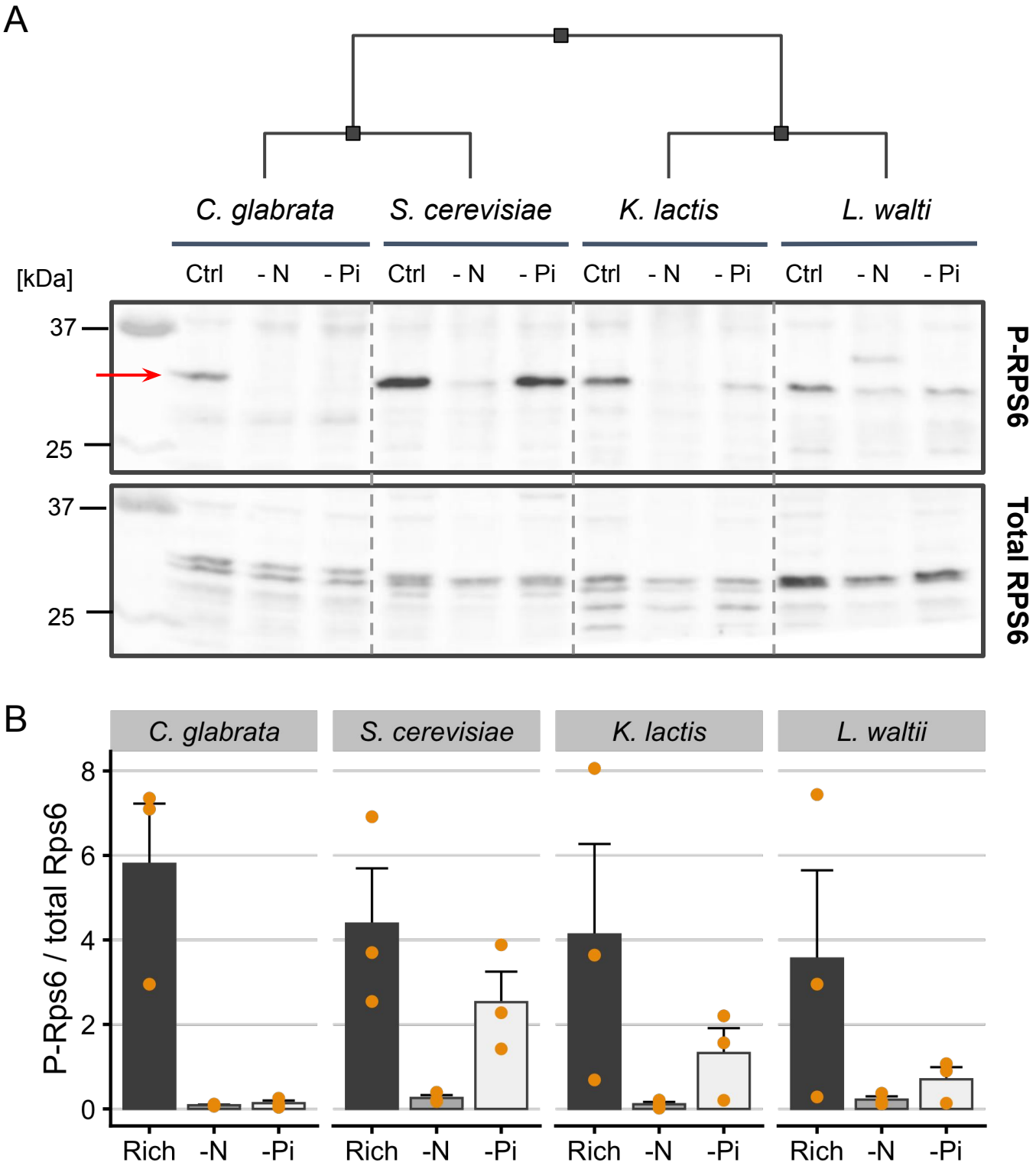

Supplementary Figure 7. TORC1 inhibition by phosphate and nitrogen starvation in diverse yeasts. (A) The tree (cladogram) on the top shows the evolutionary relationships between the different yeasts; the Western Blot image below is one of the replicates probing the P-Rps6 (top) and total Rps6 (bottom) levels in log phase *C. glabrata, S. cerevisiae, K. lactis* and *L. walti* cells grown in rich, nitrogen starvation (-N) and phosphate starvation (-Pi) media for 1 hr at 30 °C. The arrow on the top blot indicates the band for the P-Rps6. (B) Quantification of the ratio of P-Rps6 to total Rps6 based on three replicates. While the trend was obvious, the small sample size (3) limited the power of a paired Student's t-test used to compare the starvation conditions to the rich condition in each species, which resulted in *P*-values that were not significant at a 0.05 level after Bonferroni correction.

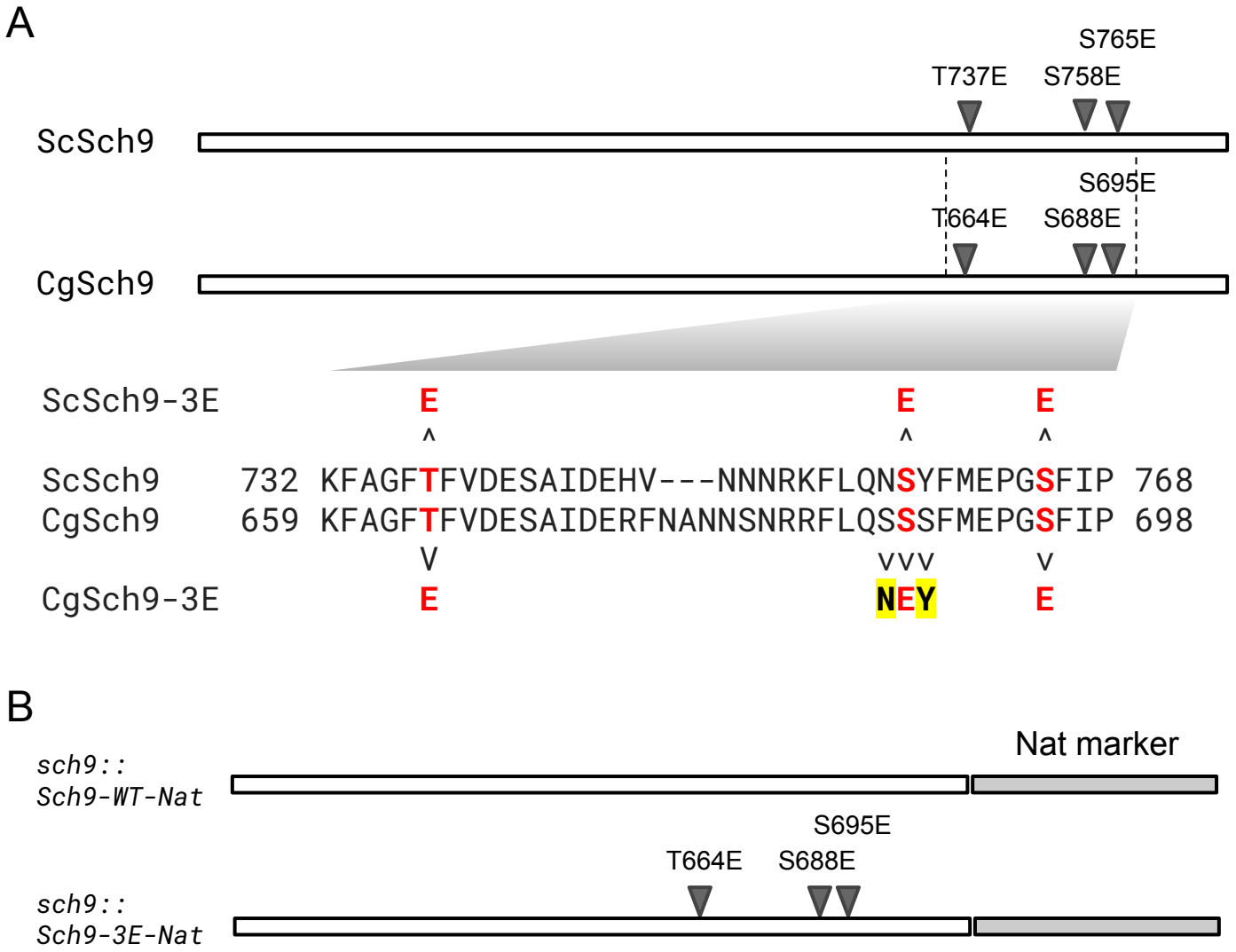

Supplementary Figure 8. Sch9-3E phosphomimetic mutant in *C. glabrata*. (A) Schematic alignment of Sch9 protein in *S. cerevisiae* and *C. glabrata*. The three TORC1 targeted S/T sites in ScSch9, based on Urban *et al.* 2007, and the corresponding sites in the orthologous CgSch9 based on the alignment were labeled with a triangle and the mutations were labeled on the top. The region containing the three S/T sites were shown below as a pairwise sequence alignment below. The S/T sites were shown in red bold fonts. For the second site, S758 (in ScSch9), the corresponding site in CgSch9 are flanked by two serines, making it difficult to determine whether and which serine may be the authentic phosphorylation site. We therefore decided to make three mutations to turn the site into the same sequence as in the ScSCH9-3E mutant. (B) To replace the endogenous *SCH9* gene in *C. glabrata* with the mutant alleles, we added an antibiotic Nat marker at the end of either the wild type *CgSCH9* gene or the *CgSCH9-3E* allele and performed allele swaps. The first construct provides a control for the effect of disrupting the 3' UTR by adding the Nat marker.

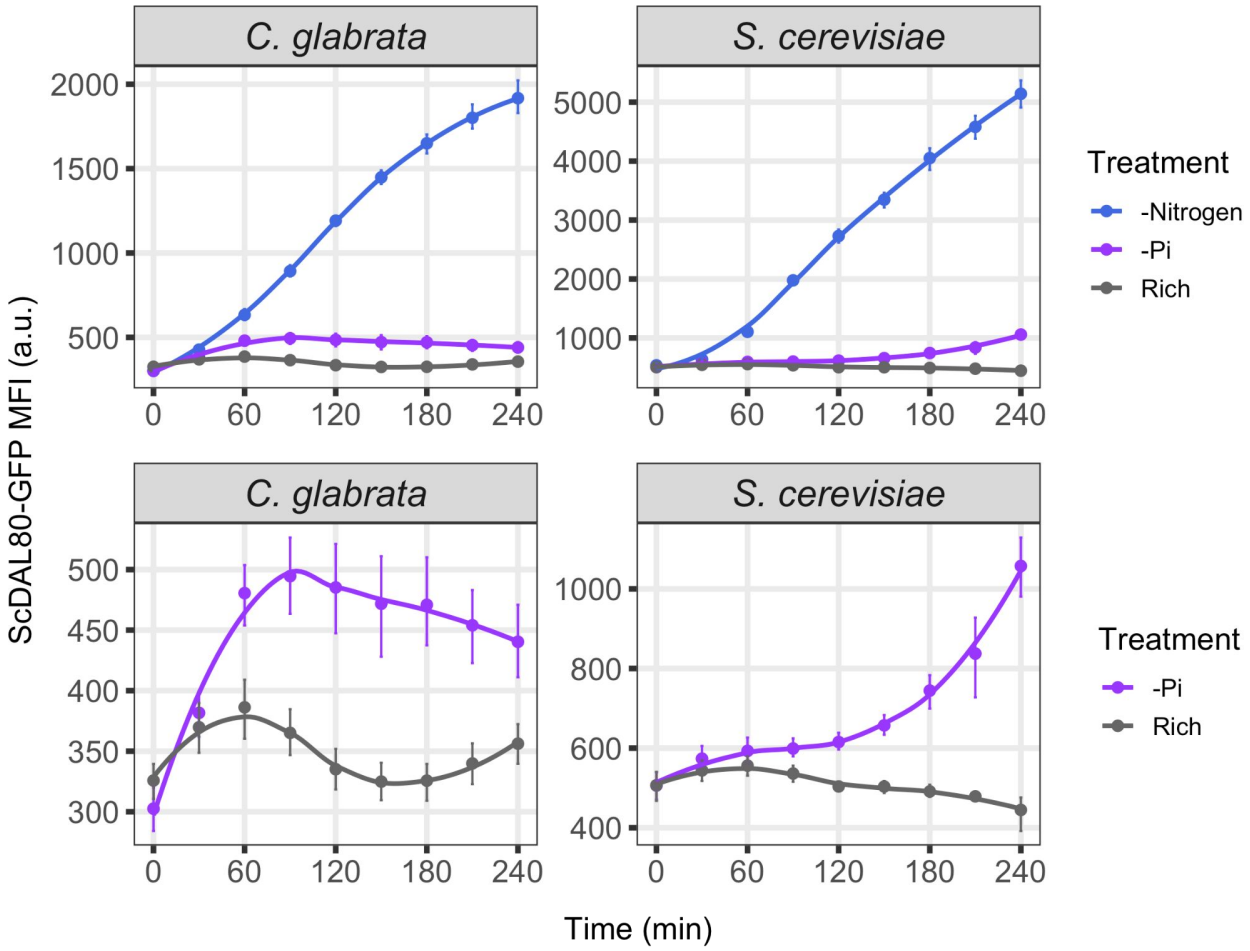

Supplementary Figure 9. *DAL80* induction kinetics under nitrogen and phosphate starvation in *S. cerevisiae* and *C. glabrata*. ScDAL80pr-GFP expression levels were monitored via flow cytometry over a time course of 4 hours during nitrogen (-N) or phosphate starvation (-Pi) and rich medium conditions. Dots represent the mean of Median Fluorescent Intensity from > 3 biological replicates; the error bars represent the 95% CI based on 1000 bootstraps. The lines are LOESS fit to the means. The top row shows all three conditions while the bottom row shows only -Pi and Rich to better visualize the induction under -Pi.

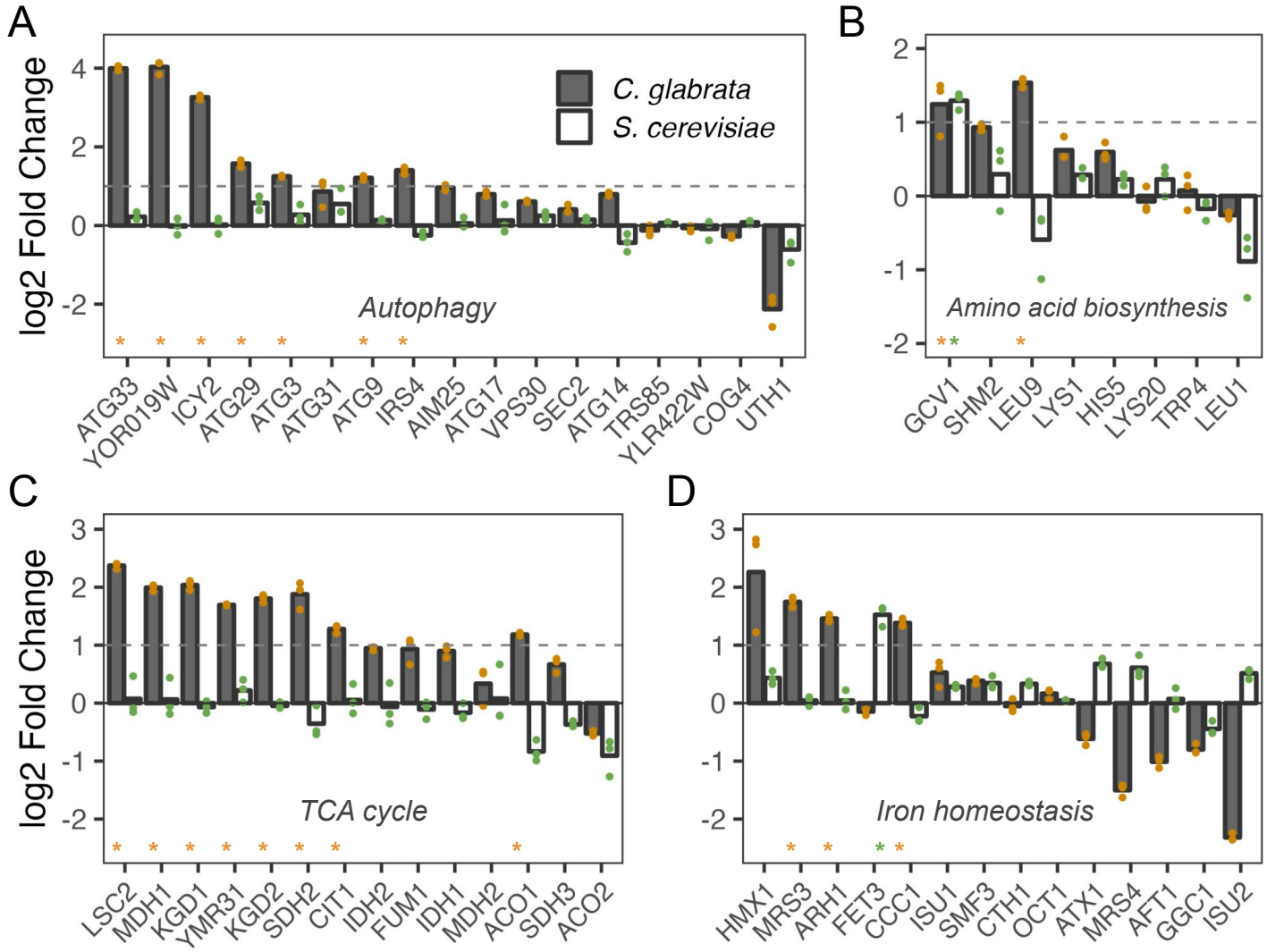

Supplementary figure 10. Genes induced after being engulfed by macrophages are also induced by a short-term phosphate starvation in *C. glabrata*. Data and plots are similar to Figure 2C-F. Gene sets were based on (Rai *et al.* 2021) supplementary figures 2 and 3 for figure 1. Gene names were based on *S. cerevisiae*. An asterisk meant the gene was significantly induced in the species at an FDR of 0.05.

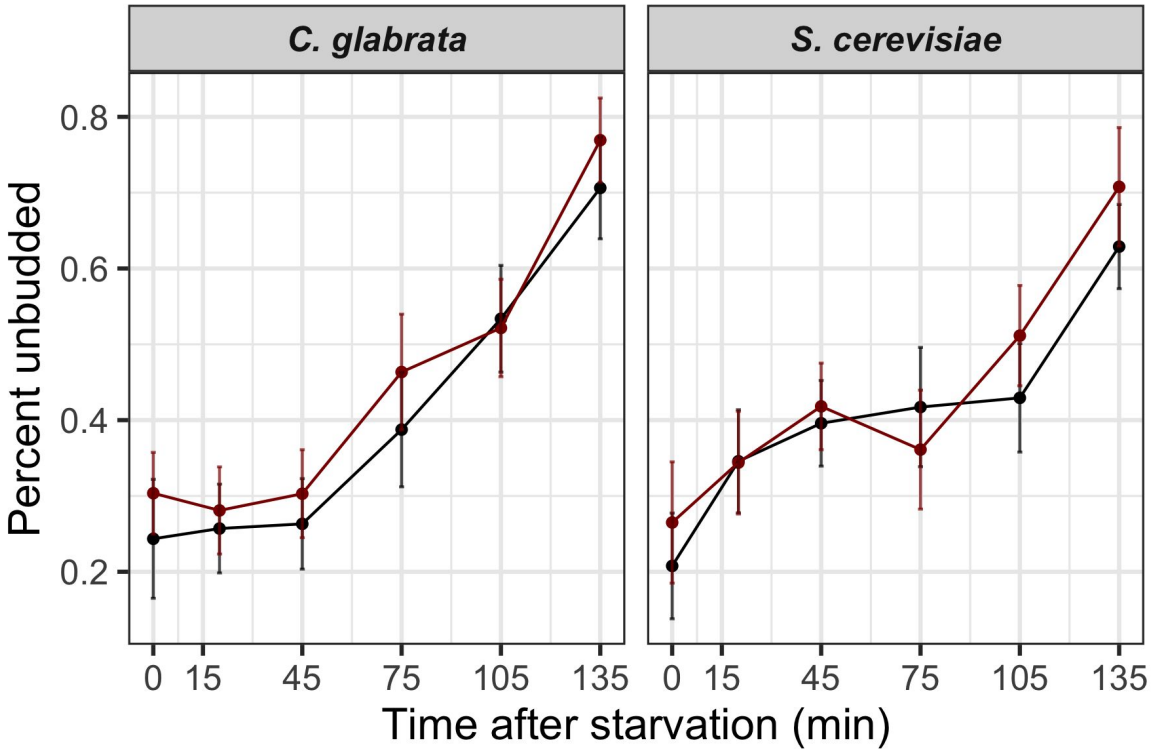

Supplementary Figure 11. Percent unbudded cells during phosphate starvation time course. Cells were taken at 0, 20, 45, 75, 105 and 135 minutes during the time course and assayed for cell morphology by light microscopy (Materials and Methods). The black and dark red dots and lines represent two biological replicates. The dots are the percentage of unbudded cells from >100 total cells examined. The error bars are the 95% confidence interval for the binomial proportion based on normal approximation (Wald Interval).